Research

New Phytologist

Flavodiiron proteins associate pH-dependently with the thylakoid membrane for ferredoxin-1-powered O_2 photoreduction

Lauri Nikkanen[1], Serhii Vakal[2], Michal Hubáček[1], Anita Santana-Sánchez[1], Grzegorz Konert[1], Yingying Wang[3], Marko Boehm[4], Kirstin Gutekunst[3,4], Tiina A. Salminen[2] and Yagut Allahverdiyeva[1]

[1]Molecular Plant Biology, Department of Life Technologies, University of Turku, Turku, FI-20014, Finland; [2]Faculty of Science and Engineering, Structural Bioinformatics Laboratory and InFLAMES Research Flagship Center, Åbo Akademi University, Turku, FI-20520, Finland; [3]Botanical Institute, Plant Cell Physiology and Biotechnology, University of Kiel, Kiel, D-24118, Germany; [4]Molecular Plant Physiology, University of Kassel, Kassel, D-34132, Germany

Author for correspondence:
Yagut Allahverdiyeva
Email: allahve@utu.fi

Received: *11 November 2024*
Accepted: *10 March 2025*

New Phytologist (2025) **246:** 2084–2101
doi: 10.1111/nph.70114

Key words: cyanobacteria, flavodiiron proteins, photosynthesis, photosynthetic regulation, proton motive force.

Summary

- Flavodiiron proteins (FDPs) catalyse light-dependent reduction of oxygen to water in photosynthetic organisms, creating an electron sink on the acceptor side of Photosystem I that protects the photosynthetic apparatus. However, ambiguity about the electron donor(s) remains, and the molecular mechanisms regulating FDP activity have remained elusive.
- We employed spectroscopic and gas flux analysis of photosynthetic electron transport, bimolecular fluorescence complementation assays for *in vivo* protein–protein interactions in the model cyanobacterium *Synechocystis* sp. PCC 6803, and *in silico* surface charge modelling.
- We demonstrated that ferredoxin-1 interacts with Flv1, Flv2, and Flv3, and is the main electron donor to FDP heterooligomers, which are responsible for the photoreduction of oxygen. Moreover, we revealed that FDP heterooligomers dissociate from the thylakoid membrane upon alkalisation of the cytosol, providing the first *in vivo* evidence of a self-regulatory feedback mechanism allowing dynamic control of FDP activity and maintenance of photosynthetic redox balance in fluctuating environments.
- Our findings have direct implications for rationally directing electron flux towards desired reactions in biotechnological applications.

Introduction

Oxygenic photosynthetic organisms, including cyanobacteria, green algae, and nonangiosperm land plants, possess class C flavodiiron proteins (FDPs). These enzymes catalyse light-dependent reduction of O_2 to H_2O through a process known as the Mehler-like reaction. This reaction creates a strong electron sink on the acceptor side of Photosystem I (PSI) and alleviates excessive reduction in the photosynthetic electron transport chain (PETC), protecting the photosynthetic apparatus from photodamage. It has been proposed that, unlike in the Mehler reaction, no harmful reactive oxygen species are produced and O_2 is reduced directly to H_2O (Vicente *et al.*, 2002). Indeed, the Mehler-like reaction is essential for the growth of cyanobacteria (Allahverdiyeva *et al.*, 2013), unicellular algae (Chaux *et al.*, 2017; Jokel *et al.*, 2018), and moss (Gerotto *et al.*, 2016) in conditions mimicking natural fluctuations of light intensity. Flavodiiron proteins are also common in nonphotosynthetic bacteria, archaea, and eukaryotes, and are classified into classes A–H depending on their domain composition (Folgosa *et al.*, 2018). All FDPs share a core modular domain structure containing a metallo β-lactamase-like domain with a nonheme diiron catalytic site and a flavodoxin-like domain with a flavin mononucleotide-binding site. Flavodiiron proteins in photosynthetic organisms typically also harbour a C-terminal flavin-binding domain with predicted NAD(P)H:flavin oxidoreductase activity (Folgosa *et al.*, 2018). Some FDPs, including those in photosynthetic algae, catalyse the reduction of nitric oxide (NO) to nitrous oxide, while yet others can reduce both NO and O_2 (Folgosa *et al.*, 2018; Burlacot *et al.*, 2020; Blomberg & Ädelroth, 2023).

The model cyanobacterium *Synechocystis* sp. PCC 6803 (hereafter *Synechocystis*) has four FDP isoforms: Flv1 (*sll1521*), Flv3 (*sll0550*), Flv2 (*sll0219*), and Flv4 (*sll0217*) (Helman *et al.*, 2003) that likely form various homo- and heterooligomeric conformations. The Mehler-like reaction is catalysed by heterooligomers consisting of Flv1 and Flv3 or Flv2 and Flv4 (Helman *et al.*, 2003; Allahverdiyeva *et al.*, 2013; Shimakawa *et al.*, 2015; Mustila *et al.*, 2016; Santana-Sanchez *et al.*, 2019). Although it has been established that FDPs function as a release valve for excessive electrons on the acceptor side of PSI (Helman *et al.*, 2003; Allahverdiyeva *et al.*, 2013; Santana-Sanchez *et al.*, 2019), and that the Mehler-like reaction is dependent on the presence of all four FDPs under air-level CO_2 (Mustila *et al.*, 2016; Santana-Sanchez *et al.*, 2019), consensus about the identity of the electron donor(s) to FDPs has remained elusive. Based on the presence of the C-terminal NAD(P)H: flavin

oxidoreductase-like domain and *in vitro* experiments with recombinant proteins, it was suggested that NAD(P)H would function as the main electron donor to Flv1, Flv3, and Flv4 (Vicente *et al.*, 2002; Shimakawa *et al.*, 2015; Brown *et al.*, 2019). However, in those experiments FDPs were present as homooligomers, whose physiological function remains unknown but has been shown to be distinct from O_2 photoreduction (Mustila *et al.*, 2016). Given the distinct kinetic profiles of O_2 photoreduction catalysed by Flv1/3 and Flv2/4 heterooligomers under air-level CO_2 concentrations (Santana-Sanchez *et al.*, 2019), the *in vivo* electron donor to different heterooligomers, and to the unknown reactions catalysed by FDP homooligomers, could differ. Flv1, Flv2, Flv3, and Flv4 homodimers, as well as Flv2/4 heterodimers have been biochemically detected in *Synechocystis*, and the formation of tetramers of recombinant Flv3 in *E. coli* has been observed (Allahverdiyeva *et al.*, 2011; Zhang *et al.*, 2012; Mustila *et al.*, 2016). However, Flv1/3 heterooligomers have not been directly observed, and the abilities of FDPs to interact with each other and to form different heterodimers and higher-order oligomers have not been fully explored.

Alternative electron donors, such as ferredoxin (Fed) or ferredoxin:$NADP^+$ oxidoreductase (FNR), were not tested in the aforementioned *in vitro* studies (Vicente *et al.*, 2002; Brown *et al.*, 2019). There are two FNR isoforms in *Synechocystis*: the larger FNR_L form functions as the main photosynthetic carrier of electrons from Fed to $NADP^+$, while the smaller FNR_S form, deriving from later initiation of transcription of the *petH* gene, is upregulated under nutrient starvation or in heterotrophic conditions (Thomas *et al.*, 2006). The FNR was recently suggested to catalyse NADPH oxidation during cyclic electron transport (CET) upon dark–light transitions, providing reduced Fed for NDH-1 (Miller *et al.*, 2022). However, *in vivo* measurements of light-induced NAD(P)H and Fed redox changes in wild-type (WT) *Synechocystis* and Flv1/3-deficient mutant cells strongly support Fed as the main electron donor at least to Flv1/3 heterooligomers, with uncertainty persisting about the donor to Flv2/4 (Nikkanen *et al.*, 2020; Sétif *et al.*, 2020). Moreover, as the Fed signal in the near-infrared (NIR) absorbance spectroscopy method is affected by the PSI iron–sulphur clusters, direct electron transfer between Flv1/3 could not be excluded (Sétif *et al.*, 2020). *Synechocystis* has 11 Fed isoforms (Fed1-Fed11; Artz *et al.*, 2020), but only little is known about their specific functions or the extent of redundancy between them. Fed1–6, as well as Fed10–11, are 'plant-type' Feds harbouring a [2Fe-2S] cluster, while Fed7, 8, and 9 are bacterial types with [4Fe-4S], [3Fe-4S] [4Fe-4S], and [4Fe-4S] [4Fe-4S] iron–sulphur cluster compositions, respectively (Cassier-Chauvat & Chauvat, 2014; Artz *et al.*, 2020; Wang *et al.*, 2022). Previously, Fed9 has indeed been shown to interact with Flv3 in a bacterial two-hybrid system (Cassier-Chauvat & Chauvat, 2014), and Flv1 and Flv3 with Fed1 in a Fed-affinity chromatographic assay (Hanke *et al.*, 2011). Moreover, the Δ*fed7* mutant has a lowered expression level of the *flv4-2* operon and decreased photosynthetic efficiency under high irradiance and air-level [CO_2] (Mustila *et al.*, 2014). Evidence of *in vivo* interaction is, however, lacking.

To reveal whether any of the low-abundance Fed isoforms in *Synechocystis* (Fed2-Fed11), NADPH, or FNR are required for the Mehler-like reaction, we performed biophysical characterisation of deletion strains deficient in low-abundance Feds and FNR. We also developed a bimolecular fluorescence complementation (BiFC) platform to study protein–protein interactions in living cyanobacterial cells, which we then utilised to examine the capability of FDPs to interact *in vivo* with putative electron donors and with each other. The BiFC takes advantage of the reassembly of a fluorescent protein (FP) upon proximity of two co-expressed fusion proteins consisting of a protein of interest and an N- or C-terminal fragment of an FP (Hu *et al.*, 2002; Kerppola, 2008). The FP is then excited at the appropriate wavelength, and the resulting fluorescence emission from interactions is typically detected by a confocal microscope. A substantial benefit of BiFC tests in comparison with *in vitro* methods, such as co-immunoprecipitation, or methods based on exogenous expression, such as two-hybrid systems, is that it can also provide information on the *in vivo* subcellular localisation of the detected protein–protein interactions. Although BiFC has been extensively used to study interactions in plant cells and chloroplasts, as well as in other bacterial species (Walter *et al.*, 2004; Kerppola, 2008; Kudla & Bock, 2016; Nikkanen *et al.*, 2016), it has not, to the best of our knowledge, been previously utilised in cyanobacteria. Background fluorescence caused by cyanobacterial phycobilisomes or Chl does not, however, interfere with the use of fluorophores, such as green fluorescence protein (GFP), yellow fluorescence protein (YFP), or cyan fluorescence protein (CFP) (Yokoo *et al.*, 2015).

Our combined approach of biophysical characterisation and BiFC assays allowed us to demonstrate that Fed1, not NADPH or FNR, is likely to be the main electron donor to the light-induced Mehler-like reaction catalysed by Flv1/3 and Flv2/4 heterooligomers. Moreover, the subcellular localisation of the interactions between FDPs and Fed1 provided evidence that dynamic changes in cytosolic pH control the reversible association of different Flv1/3 and Flv2/4 heterooligomers with the thylakoid membrane. *In silico* modelling of FDP heterooligomer surface charges supported pH-dependent electrostatic binding to thylakoid membranes. Based on these findings, we propose a novel self-feedback mechanism for precise post-translational regulation of Fed1-driven O_2 photoreduction activity of FDP heterooligomers.

Materials and Methods

Construction of mutants and culture conditions

To create BiFC strains, we aimed to reduce false positives from overexpressed proteins in confined cyanobacterial cells (Kudla & Bock, 2016) by using a Venus YFP variant with an I152L mutation to decrease self-reassembly (Kodama & Hu, 2010). Proteins of interest were fused to the N or C terminus of the Venus fragment via a short linker for flexibility and then co-expressed under isopropyl b-D-1-thiogalactopyranoside (IPTG)-inducible lac2 promoters and S3 ribosome binding sites of the *cpcB* gene on a single pDF-lac2 plasmid to ensure strong YFP expression (Thiel *et al.*, 2018; Supporting Information Fig. S1). Coding

sequences of the *Synechocystis* sp. PCC 6803 genes and Venus YFP fragments (VN and VC; Kodama & Hu, 2010) were synthetised by GenScript (Piscataway, NJ, USA). Modular cloning details are found in Methods S1.

Gene fragments *fed10* (*sll1584*) and *fed11* (*ssl3044*) (Artz *et al.*, 2020) along with flanking regions and a kanamycin resistance cassette (Table S1) were PCR-amplified. Constructs were generated by Gibson cloning (Gibson *et al.*, 2009) to integrate the fragments into the pBluescript SK(+) vector, followed by plasmid sequencing and transformation into *Synechocystis* cells (Williams, 1988). Transformants were checked by PCR after several rounds of segregation (Fig. S2a).

The strains used included the glucose-tolerant *Synechocystis* sp. PCC 6803 WT (Williams, 1988), mutant strains ΔFed2/Fed2, ΔFed3, ΔFed4, ΔFed5/Fed5, ΔFed6, ΔFed7Fed8Fed9, ΔFed9 (Wang *et al.*, 2022), the ΔFlv3 strain (Helman *et al.*, 2003), the ΔNdhD1NdhD2 (ΔD1D2) strain (Ohkawa *et al.*, 2000), the ΔFlv3 D1D2 strain (Nikkanen *et al.*, 2020) as well as the ΔFNR_L (FSI) and ΔFNR_S (MI6) strains, deficient in the large and small isoform of FNR, respectively (Thomas *et al.*, 2006).

Pre-experimental cultures were grown in 30 ml of BG-11 medium (pH 7.5) with agitation at 30°C, 3% [CO_2] and continuous white light (50 μmol photons m^{-2} s^{-1}). Mutant precultures included appropriate antibiotics. For physiological experiments, cells were harvested at the logarithmic phase, resuspended in antibiotics-free BG-11 at OD_{750} = 0.2, then transferred to air-level or 3% [CO_2], 30°C, and grown continuously under white light (50 μmol photons m^{-2} s^{-1}). See 'BiFC tests' in this section for the growth conditions of BiFC experiments.

Membrane-inlet mass spectrometry

Exchange of $^{16}O_2$ (*m/z* = 32) and $^{18}O_2$ (*m/z* = 36) was measured *in vivo* with membrane-inlet mass spectrometry (MIMS) as in Mustila *et al.* (2016). After harvesting, cells were resuspended in fresh BG-11 (pH 7.5) at 10 μg Chl ml^{-1} and acclimated for 1 h in air [CO_2] under 50 μmol photons m^{-2} s^{-1}. Cells were then supplemented with $^{18}O_2$, 1.5 mM $NaHCO_3$, dark-adapted for 15 min, and O_2 exchange was monitored under 500 μmol photons m^{-2} s^{-1} white actinic light for 5 min. O_2 exchange rates were calculated as per Beckmann *et al.* (2009).

BiFC tests

The BiFC strains were grown in BG-11 (pH 7.5) with 35 μg ml^{-1} of chloramphenicol and 50 μg ml^{-1} of spectinomycin at 30°C under 3% [CO_2] and continuous 50 μmol photons m^{-2} s^{-1} of white light until OD_{750} 0.5. OD_{750} was adjusted to 0.25 with standard fresh BG-11 (pH 7.5) without antibiotics, BG-11 without Mg^{2+} or Ca^{2+}, or BG-11 with 25 mM $MgCl_2$ and 30 mM $CaCl_2$. Cultures were supplemented with 1 mM IPTG to induce BiFC protein expression and grown, harvested, and resuspended in 2 ml of fresh BG-11. Venus fluorescence and Chl autofluorescence were imaged with a Zeiss LSM880 confocal microscope with at 488 and 543 nm excitation and detection at 517–597 nm (for Venus) and 651-758 nm (for Chl). [Correction added on 8 May 2025, after first online publication: the detection values in the preceding sentence have been corrected.] 30 μM carbonyl cyanide m-chlorophenylhydrazone (CCCP), 20 μM nigericin, 20 μM DCMU, or 40 μM valinomycin was added as needed. Fluorescence co-localisation was analysed using the Fiji software with the EzColocalization plugin (Stauffer *et al.*, 2018) and a custom script (available at GitHub: https://github.com/gekoneCAC/CellHorizontalProfile). Negative controls included BiFC tests with empty vectors (e.g. Flv2-VC+ unfused VN), which emitted low Venus fluorescence in the cyanobacterial system (Fig. S3).

NAD(P)H fluorescence and near-infrared spectrophotometry

NAD(P)H fluorescence changes (420–580 nm) were measured using a Dual-PAM 100 spectrophotometer with the 9-AA/NADPH module (Walz; Schreiber & Klughammer, 2009). Cells were harvested, resuspended in fresh BG-11 at 5 μg Chl*a* ml^{-1}, and dark-adapted for 15 min. Fluorescence was recorded under 500 μmol photons m^{-2} s^{-1} for 40 s, followed by 40 s in darkness.

In vivo redox changes in P700, PC, and Fed were deconvoluted from absorbance differences at four NIR wavelengths (780–820, 820–870, 840–965, and 870–965 nm) with a DUAL-KLAS-NIR spectrophotometer (Walz) (Klughammer & Schreiber, 2016). The differential model plot (DMP) used to deconvolute the Fed signal was measured from ΔFlv3 D1D2 triple mutant cells (Nikkanen *et al.*, 2020), while P700 and PC DMPs were determined as described by Theune *et al.* (2021). Cells were harvested, resuspended in BG-11 at 20 μg Chl*a* ml^{-1}, and dark-adapted for 15 min. Cells were illuminated for 3 s (3000 μmol photons m^{-2} s^{-1}) with a saturating pulse after 200 ms to reduce the Fed pool, followed by 4 s of darkness, and far-red (FR) light for 10 s with a saturating pulse at the end to fully oxidise P700 and PC. The maximum reduction and oxidation values were used to normalise the traces.

Electrochromic shift measurements

Light-induced changes in the proton motive force (*pmf*), thylakoid conductivity (gH+), and proton flux (vH+) were determined by monitoring the dark interval relaxation kinetics of the 500–480 nm absorbance difference, representing the electrochromic shift (ECS) in *Synechocystis* (Viola *et al.*, 2019; Nikkanen *et al.*, 2020). Cells were harvested and resuspended in fresh BG-11, low cation BG-11, or high cation BG-11 (pH 7.5) at 7.5 μg ml^{-1} Chl. Suspensions were illuminated at 500 μmol photons m^{-2} s^{-1} with 600 ms dark intervals and absorbance changes were detected using a JTS-10 spectrophotometer (BioLogic, France) with appropriate filters (Edmund Optics, Barrington, NJ, USA).

Acridine orange and acridine yellow fluorescence measurements

To monitor light-induced alkalisation of the cytosol, acridine orange (AO) and acridine yellow (AY) fluorescence changes (Teuber *et al.*, 2001) were recorded using a Dual-PAM-100

spectrophotometer with the AO/AY module (Schreiber & Klughammer, 2009). Cells were grown in air-level CO_2 in BG-11 (pH 7.5) under 50 µmol photons m^{-2} s^{-1} for 4 d, harvested, and suspended in fresh BG-11 at 5 µg ml^{-1} Chl. Cells were treated with 5 µM AO or AY and 1 mM potassium cyanide (KCN) (as needed), followed by 10 min dark adaptation before measurements at 216 or 500 µmol photons m^{-2} s^{-1}, as specified.

Immunoblotting

Total proteins were extracted from BiFC cultures for microscopy as described by Zhang *et al.* (2009). For FDP subcellular localisation, WT *Synechocystis* cells were grown for 4 d under 50 µmol photons m^{-2} s^{-1} at 30°C in air-level [CO_2]. Samples were taken from light, dark-adapted for 20 min, or light-supplemented with 30 µM CCCP, and then frozen in liquid N_2. Soluble and membrane fractions were isolated as described by Zhang *et al.* (2009). Proteins were separated by SDS-PAGE on 4–15% Mini-Protean TGX 4–15% gels (Bio-Rad) and transferred to polyvinylidene fluoride (PVDF) membranes. Membranes were probed with antibodies against the N-terminal fragment of YFP (Origene, Rockville, MD, USA), Flv1 and Flv4 (Genscript, Piscataway, NJ, USA), Flv2 and Flv3 (Antiprot, Puchheim, Germany), and PetH (kindly shared by H. Matthijs). Horseradish peroxidase (HRP)-conjugated goat-anti mouse (Bio-Rad) and goat-anti-rabbit (GE Healthcare, Chicago, IL, USA) secondary antibodies as well as Enhanced Chemiluminesence, ECL (Amersham, Buckinghamshire, UK) were used for detection.

In silico modelling

The sequences of *Synechocystis* Flv1, Flv2, Flv3, and Flv4 proteins were retrieved from UniProt (IDs: P74373, P72723, Q55393, and P72721). Crystal structures for the multiple alignments were obtained via BLAST from the Protein Data Bank (Berman, 2000) using these sequences. The β-lactamase-like and flavodoxin domains of Flv1 (PDB: 6H0D) were superimposed on the *Methanothermobacter marburgensis* $F_{420}H_2$ oxidase structure (PDB: 2OHI, 2OHJ; Seedorf *et al.*, 2007) for sequence alignment. The 3D models for the open and closed states of Flv1, Flv2, Flv3, and Flv4 monomers, along with homooligomers (-Flv1/Flv1 and Flv3/Flv3), and heterooligomers (Flv1/Flv3 and Flv2/Flv4), were built using MODELLER v.10.4 (Webb & Sali, 2016), based on the $F_{420}H_2$ oxidase structures.

Sequence alignments were done with MALIGN (Lehtonen *et al.*, 2004) and visualised using ESPRIPT 3.0R (Robert & Gouet, 2014), and the MODELLER models were selected based on zDOPE and Molpdf scores. Model quality was assessed using the Protein Reliability Report in Schrodinger Maestro 13.3. Following protein preparation at pH 7.0 and pH 8.5 using the 'prepwizard' script, the net charges were calculated in triplicate using the 'calc_protein_descriptors' script in Schrodinger Bioluminate (Schrödinger Release 2023-1, 2021a). The electrostatic potential surfaces for FDP monomers and oligomers were visualised with the Poisson–Boltzmann ESP module in Schrodinger Maestro (Schrödinger Release 2023-1, 2021b).

YFP-labelled *Synechocystis* Flv1 and Flv3 sequences were used to model the full-length Flv1-VN/Flv3-VC complex. The heterodimers were modelled with VN and VC fragments of YFP attached to Flv1 or Flv3. The YFP structure was modelled using the AlphaFold2 Multimer Google Collab notebook (Mirdita *et al.*, 2022) with 48 recycles, pdb100 template mode, and Amber relaxation. The C-terminal flavin reductase domain of Flvs was modelled using the crystal structure of *Thermus thermophilus* putative flavoprotein (PDB: 1WGB) as a monomer template. Monomeric models were overlaid onto the dimeric structure of *T. thermophilus* probable flavoprotein HB8 [TS1] (Imagawa *et al.*, 2005; PDB: 1YOA[SV2]) to create dimers. The spatial arrangement of the flavodiiron core and the C-terminal flavin oxidase domain was predicted using ClusPro (Kozakov *et al.*, 2017). Full-length YFP-labelled models were reconstructed by combining the flavodiiron core, docked C-terminal flavin reductase domains, and AF2-modelled YFP in multiple-template modelling in MODELLER. The models underwent 500-step energy minimisation and 100-ns molecular dynamics simulations in explicit solvent with Desmond (Schrödinger, 2022) to explore interdomain loop conformations. The models with the lowest free energy were visualised using PYMOL.

Statistical analysis

Statistical analysis (Student's *t*-test and one-way ANOVA) were performed in OriginPro 2024 to determine the statistical significance of differences. One-sample *t*-tests were used to compared western blot band intensities to controls (normalised to 1). $P < 0.05$ was considered significant. Details are presented in Tables S2 and S3. Independent cultures grown for at least 4 d were biological replicates.

Results

Flv3 interacts with FNR on thylakoids, but FNR and NADPH are not the main reductants of Flv1/3 heterooligomers in the Mehler-like reaction

First, we investigated whether FDPs interact directly with, and/or are reduced by FNR. To that end, we monitored real-time NAD(P)H redox changes and light-induced O_2 exchange in ΔFNR_L and ΔFNR_S mutants (also called FSI and MI6, respectively; Thomas *et al.*, 2006). Light-dependent $NADP^+$ reduction was impaired in ΔFNR_L (Fig. 1a,b), in agreement with the previous observation of a lower NADPH/$NADP^+$ ratio (Korn *et al.*, 2009), while ΔFNR_S showed no difference from WT.

In WT cells, a strong but transient O_2 photoreduction peak occurs within the first minute of illumination, primarily driven by Flv1/3 heterooligomers with some contribution from Flv2/4, while sustained O_2 photoreduction is mainly dependent on Flv2/4 (Santana-Sanchez *et al.*, 2019; Fig. 1c). If NADPH served as the electron donor for FDP heterooligomers, the shortage of light-induced NADPH in ΔFNR_L cells would be expected to inhibit the Mehler-like reaction. However, no major impairment in maximal O_2 photoreduction rate was detected in either ΔFNR_L or ΔFNR_S

New Phytologist

when O_2 fluxes were monitored by time-resolved MIMS (Fig. 1c,d). A small decrease in maximum O_2 photoreduction in ΔFNR_L likely results from reduced Flv2 protein levels in the mutant (Fig. 1e), as Flv2/4 deficiency partially impairs the Mehler-like reaction under air-level [CO_2] conditions (Santana-Sanchez *et al.*, 2019). Conversely, slightly elevated protein levels of Flv1 and Flv3 were detected in both FNR mutants, albeit significantly only in ΔFNR_S (Fig. 1e). To determine whether the lower Flv2/4 level caused the decreased O_2 photoreduction in ΔFNR_L, MIMS experiments were repeated under elevated (3%) [CO_2], where the *flv4-2* operon is not expressed (Zhang *et al.*, 2009). Indeed, under these conditions, ΔFNR_L showed no difference to WT in O_2 photoreduction rate (Figs 1c,d, S4d). Despite being slightly higher under elevated [CO_2] than the ambient levels, the light-induced accumulation of NADPH was notably impaired in ΔFNR_L cells under both conditions, while no difference to WT was observed in ΔFNR_S (Fig. S5a,b). In low-light conditions where the Mehler-like reaction activity is low (Allahverdiyeva *et al.*, 2013; Ortega-Martínez *et al.*, 2024), NADPH accumulation in ΔFNR_L was also notably lower than in WT (Fig. S5c,d). As no significant difference was detected in the NAD(P)H fluorescence intensity in dark-adapted cells (Fig. S5e), the impaired light-induced NADPH generation in ΔFNR_L cells was not caused by a more reduced $NADP^+$/NADPH pool in the dark. Slightly elevated NAD(P)H dark fluorescence was detected in ΔFNR_S (Fig. S5e).

An elevated level of dark respiration was detected in air-grown ΔFNR_L cells (Fig. S4c), possibly due to the increased amount of FNR_S (Fig. 1f; Thomas *et al.*, 2006). No significant differences in maximal gross O_2 evolution (Fig. S4b) or steady-state CO_2 fixation rate (Fig. S4e) were detected between the FNR mutants and WT.

Flv1/3 deficiency prevents re-oxidation of Fed and P700 during the first seconds of strong illumination (Nikkanen *et al.*, 2020; Sétif *et al.*, 2020; Theune *et al.*, 2021). DUAL-KLAS-NIR spectrometry analysis revealed that while ΔFlv3 cells failed to re-oxidise Fed, PC, and P700 after initial reduction,

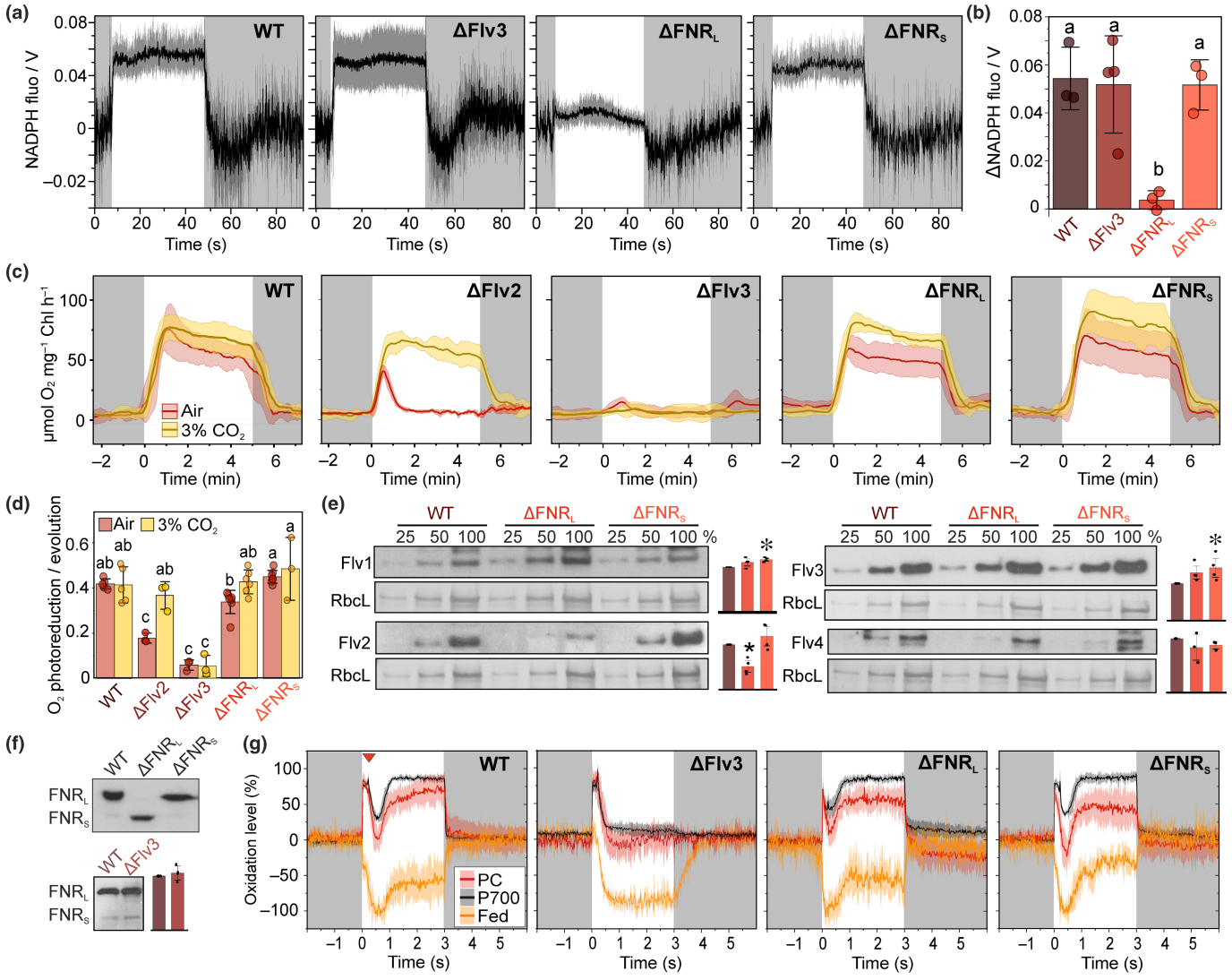

Fig. 1 Photosynthetic characterisation of *Synechocystis* ferredoxin:NADP$^+$ oxidoreductase (FNR) mutants and protein–protein interaction tests between FNR_L and flavodiiron proteins (FDPs). (a) Light-induced NAD(P)H fluorescence changes in wild-type (WT), ΔFlv3, ΔFNR_L (no FNR_L, increased amount of FNR_S), and ΔFNR_S (no FNR_S and FNR_L present) cells during preillumination darkness, followed by 40 s illumination at 500 μmol photons m^{-2} s^{-1} and subsequent darkness. Averaged traces from three (WT, ΔFNR_L, ΔFNR_S) or four (ΔFlv3) biological replicates ±SD (shadowed area) are shown. Dark-adapted NAD(P)H fluorescence levels were set to 0. (b) Quantification of light-induced change in the NAD(P)H fluorescence signal in the experiments for (a), calculated as mean fluorescence level between 30 and 40 s of illumination – mean fluorescence level in the preillumination dark period. This timeframe was chosen to coincide with the maximal activity of flavodiiron proteins (FDPs). Values are averages from three (WT, ΔFNR_L, and ΔFNR_S) or four (ΔFlv3) biological replicates ±SD with individual data points shown as circles. Statistical significance was tested by one-way ANOVA and a Tukey's *post hoc* test for comparison of means. Means that do not share a grouping letter (a, b) are significantly different ($P < 0.05$). (c) O_2 uptake kinetics measured by membrane-inlet mass spectrometry (MIMS) in WT, ΔFlv2, ΔFlv3, ΔFNR_L, and ΔFNR_S cells during 5 min illumination at 500 μmol photons m^{-2} s^{-1} and subsequent darkness. $^{18}O_2$ was added before the measurement in equal concentration to $^{16}O_2$ in order to distinguish O_2 uptake from O_2 evolution. Averaged traces from five (WT), three (ΔFlv2 and ΔFlv3), and seven (ΔFNR_L and ΔFNR_S) biological replicates ± SD (shadowed area) are shown in red from cultures grown under air-level [CO_2], and in yellow from five (WT), six (ΔFNR_L), and three (ΔFlv2, ΔFlv3, and ΔFNR_S) replicates grown under 3% [CO_2]. (d) The average magnitudes of the maximum O_2 photoreduction peaks normalised to the maximum O_2 evolution rate. Averages from five (WT), three (ΔFlv2 and ΔFlv3), and seven (ΔFNR_L and ΔFNR_S) biological replicates ±SD are shown in red from cultures grown under air-level [CO_2], and in yellow from five (WT), six (ΔFNR_L), and three (ΔFlv2, ΔFlv3, and ΔFNR_S) replicates grown under 3% [CO_2]. Individual data points are shown as circles. Statistical significance was tested by one-way ANOVA and Tukey's *post hoc* tests for comparison of means. Comparisons were made within the air-level and 3% [CO_2] sets of samples. (e) Immunodetection of Flv1, Flv2, Flv3, and Flv4 protein content in WT, ΔFNR_L, and ΔFNR_S cells using specific antibodies. Representative blots and Coomassie brilliant blue-stained band of the large subunit of Rubisco (RbcL, as loading control) from three biological replicates are shown, with bar charts showing quantification of band intensity ± SD, individual data points shown as black dots. *Denotes statistically significant difference to WT control according to one-sample Student's *t*-tests. Total proteins were extracted from cultures grown under air-level [CO_2] conditions. (f) Immunodetection of FNR protein content in WT, ΔFlv3, ΔFNR_L, and ΔFNR_S cells using specific antibodies. Representative blots from four biological replicates are shown, with the bar chart showing quantification of FNR_L band intensity in WT vs ΔFlv3 cells ± SD. Individual data points are shown as black dots. Difference to WT control was found statistically insignificant ($P > 0.05$) by a one-sample Student's *t*-test. (g) Changes of PC, P700, and ferredoxin (Fed) in WT, ΔFlv3, ΔFNR_L, and ΔFNR_S cells, as measured with a DUAL-KLAS-near-infrared (NIR) spectrophotometer. The traces are normalised to the maximal oxidation values of PC and P700 and maximal reduction of Fed, as determined with the NIRMAX protocol, of which a 3-s illumination with actinic light is shown here, including a multiple turnover pulse after 200 ms (indicated by the red triangle in the WT panel). Averaged traces from three (ΔFlv3) or five (WT, ΔFNR_L, and ΔFNR_S) biological replicates are shown, with SD as the shadowed area.

ΔFNR_L and ΔFNR_S showed WT-like re-oxidation kinetics within seconds (Fig. 1g), suggesting robust FDP activity. However, in ΔFNR_L, Fed was fully reduced within *c.* 100 ms, in contrast to *c.* 400 ms WT and ΔFNR_S, and *c.* 600 ms in ΔFlv3 (Fig. S6a), showing an electron pileup at Fed when FNR_L is missing, but which is resolved once FDPs are activated at *c.* 500 ms (Nikkanen *et al.*, 2020). Additionally, delayed P700 oxidation under FR light in ΔFNR_L (Fig. S6b) suggests increased CET.

We also investigated potential protein–protein interactions between FNR_L and FDPs using the BiFC system. Co-expression of Flv3 fused to an N-terminal Venus fragment (Flv3-VN) with FNR_L fused to a C-terminal Venus fragment (FNR_L-VC) in WT *Synechocystis* cells produced strong fluorescence at 519–570 nm upon 488 nm excitation, confirming an Flv3-FNR_L interaction (Fig. 2a). To determine subcellular localisations of interactions, we compared the intensity of Chl fluorescence, marking thylakoid membrane regions, with Venus fluorescence across cell sections. Given that thylakoid membranes in *Synechocystis* are primarily at the cell periphery, the Chl regression line forms an M-shaped pattern across cell cross-sections. We also assessed Chl and Venus fluorescence co-localisation by plotting their intensities in a cytofluorograph and calculating the Pearson correlation coefficient (PCC). Venus fluorescence from FNR_L-Flv3 interactions aligned well with Chl fluorescence, yielding an average PCC of 0.66 ± 0.17 (Fig. 2a), indicating consistent localisation of FNR_L-Flv3 to the thylakoid membrane.

No interaction was detected between Flv1-VN and FNR_L-VC (Fig. 2b), or between Flv2-VC and FNR_L-VN or FNR_S-VN (Fig. S7). All FDP + FNR BiFC strains showed strong expression of both fusion proteins (Fig. S8).

Deficiency of Fed2–11 does not impair the Mehler-like reaction

To assess how the lack of single or multiple Fed isoforms affects the Mehler-like reaction, we monitored light-induced O_2 reduction in *Synechocystis* mutants deficient in Fed3, Fed4, Fed6, Fed 7, 8, and 9, Fed9, Fed10, or Fed11. Since fully segregated mutants of Fed1, Fed2, or Fed5 cannot be obtained (Wang *et al.*, 2022), partially segregated deletion strains of Fed2 and Fed5 were studied instead. The Mehler-like reaction activity, calculated as the ratio of maximum O_2 photoreduction to gross O_2 evolution, showed no major impairment in Fed2-11 mutants (Figs 3, S2b). A slight, statistically insignificant decrease was observed in cells deficient in bacterial-type Feds (ΔFed789) and (ΔFed9), while ΔFed4 showed a slight, nonsignificant increase (Fig. 3b).

All ΔFed mutants showed WT-like redox kinetics for PC, P700, and Fed (Figs 3c, S2c, S9a) as well as pool sizes of photoreducible Fed (Fig. S9b), indicating that low-abundance Feds are not essential as primary electron donors in the Mehler-like reaction or as final acceptors from the PETC.

Fed1 interacts with Flv1, Flv2, and Flv3, but not with Flv4

Fed1, the predominant isoform involved in photosynthetic electron transfer, is essential for the survival of *Synechocystis* and a knockout mutant cannot be generated (Poncelet *et al.*, 1998; Cassier-Chauvat & Chauvat, 2014; Gutekunst *et al.*, 2014). We explored interactions between Fed1 and FDPs using the BiFC system. Co-expression of Fed1-VC with Flv1-VN in WT cells showed strong Venus fluorescence, co-localising with Chl

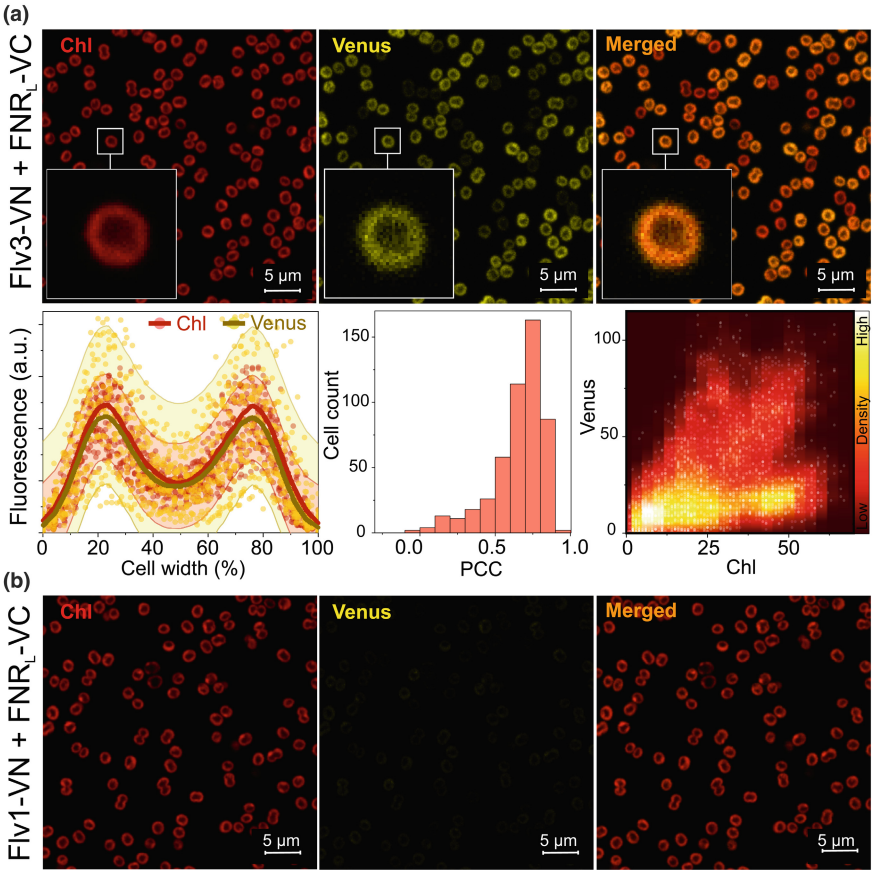

Fig. 2 Protein–protein interaction tests between FNR_L and flavodiiron proteins (FDPs) in *Synechocystis*. (a) Bimolecular fluorescence complementation (BiFC) tests between Flv3 and FNR_L and (b) Flv1 and FNR_L. Representative confocal micrographs from three independent experiments are presented, showing Chl autofluorescence emanating from the thylakoid membranes in the left panel, fluorescence from re-assembled Venus I152L fluorescent proteins in the middle, and overlaid Chl and Venus fluorescence in the right panel. The inlets show zoomed-in views of a single cell. For quantification of the subcellular localisations of the interacting fusion protein pairs, the co-localisation of Chl (red) and Venus (yellow) fluorescence is also presented with fluorescence intensities over 5-pixel-wide cross-sections of 30 cells (with width normalised to 100%) shown as a scatter plot. Red and gold lines show moving regression curves produced by locally weighted scatter plot smoothing (LOWESS) with 100 points of window. 95% confidence intervals are shown as the pale colour shadows. The histogram shows the distribution of the Pearson correlation coefficient (PCC) for Chl and Venus fluorescence co-localisation in all cells from three micrographs from individual replicates. A PCC of 1 indicates perfect co-localisation and a PCC of 0 indicates no co-localisation. The cytofluorogram shows co-localised Chl and Venus fluorescence intensities as a scatter plot. FNR, ferredoxin:$NADP^+$ oxidoreductase.

autofluorescence, indicating a Fed1-Flv1 interaction on the thylakoid membrane (Fig. 4a). By contrast, Fed1-VN with Flv3-VC showed minimal co-localisation with Chl fluorescence, indicating a cytosolic interaction (Fig. 4b). A similar result was also obtained with the reverse Venus fragment orientation (Flv3-VN + Fed1-VC; Fig. S10). Interestingly, Fed1-VN interacted with Flv2-VC in the cytosol (Fig. 4c) but not with Flv4-VN (Fig. 4d), suggesting that Flv2/4 heterooligomers may receive reducing power from Fed1, interacting specifically via Flv2.

Building on the reported two-hybrid interaction between Fed9 and Flv3 (Cassier-Chauvat & Chauvat, 2014) and the minor, nonsignificant decrease in O_2 photoreduction in ΔFed9 (Fig. 3b), we investigated *in vivo* interactions between Fed9 and Flv1 or Flv3. We detected thylakoid-localised interaction for Flv1-VN with Fed9-VC (Fig. S11a) and mixed-localisation for Flv3-VN with Fed9-VC (Fig. S11b), suggesting a possible minor or redundant role for Fed9 in electron transfer with Flv1/Flv3 heterooligomers or Flv1 or Flv3 homooligomers.

Flv1/3 and Flv2/4 interactions exhibit pH-dependent association with the thylakoid membrane

Interactions between the FDP heterooligomer pairs, Flv1-VN and Flv3-VC (Fig. 5a), and Flv4-VN and Flv2-VC (Fig. 5b), were predominantly localised in the cytosol, but in smaller subpopulations of cells, these interactions were also found at the thylakoids (Figs 5a,b, S12). This may indicate that the associations of Flv1/3 and Flv2/4 heterooligomers with the thylakoid membrane may depend on the cell's physiological state. We previously hypothesised that reversible membrane association, which may regulate FDP heterooligomer participation in O_2 photoreduction, could be influenced by changes in cytosolic pH or *pmf* which consists of transmembrane delta pH and electric potential component $\Delta\psi$ (Nikkanen *et al.*, 2021b), or cation concentrations (Zhang *et al.*, 2012). To test this, we examined the localisation of FDP isoform interactions in media with different Mg^{2+} and Ca^{2+} concentrations, and in the presence of the proton gradient uncoupler CCCP. Measurement of the 500–480 nm ECS signal (Viola *et al.*, 2019) confirmed that 30 µM CCCP effectively diminished the *pmf* and elevated the proton conductivity of the thylakoid membrane while only moderately affecting photosynthetic proton flux (Fig. S13). The initial *pmf* generation during dark-to-light transitions was lower in low-cation medium due to reduced proton flux (Fig. S14). Dissipation of the *pmf* by CCCP increased thylakoid localisation of both Flv1/3 (Fig. 5c) and Flv2/4 interactions (Fig. 5D), with the average PCC with Chl rising from 0.09 ± 0.01 (SEM) to 0.37 ± 0.01 for Flv1/3 and from 0.06 ± 0.01 to 0.33 ± 0.01 for Flv2/4.

Similar results were observed with nigericin, which by acting as a H^+/K^+ exchanger, specifically dissipates the proton gradient and delays cytosolic alkalisation, as confirmed by an AO fluorescence (Fig. S15). In the presence of 20 µM nigericin, the average

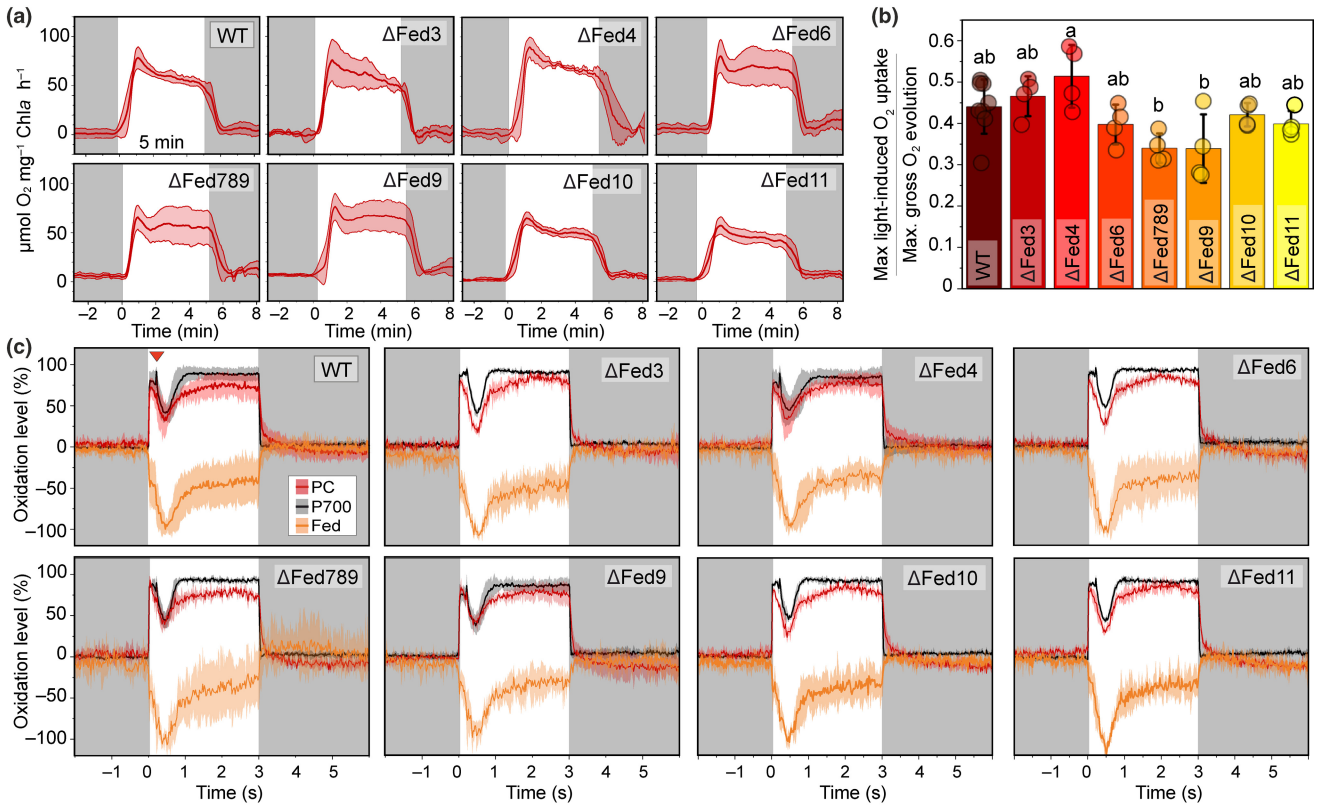

Fig. 3 Effect of low-abundance ferredoxins (Fed) on the Mehler-like reaction in *Synechocystis*. (a) O_2 photoreduction in cells deficient in low-abundance Fed isoforms. O_2 gas exchange was monitored by membrane-inlet mass spectrometry (MIMS) before, during, and after 5 min of illumination with strong actinic light (500 µmol photons m^{-2} s^{-1}). Averaged traces from eight (wild-type (WT)) or four (ΔFed3, ΔFed6, ΔFed789, ΔFed10, ΔFed11, ΔFed4, and ΔFed9) biological replicates with SD are shown. (b) Averages with SD of peak O_2 photoreduction rate at *c.* 30 s of illumination normalised to the maximum gross rate of O_2 evolution. Data are averages from four or eight biological replicates as in (a) and individual data points are shown as circles. Statistical significance of differences is indicated by lowercase letters according to one-way ANOVA and Tukey's *post hoc* test for comparison of means, with $P < 0.05$ considered significant. (c) Redox changes of plastocyanin (PC), P700, and Fed in WT and Fed mutant cells. PC, P700, and Fed redox changes are measured with a DUAL-KLAS-NIR spectrophotometer. The traces are normalised to the maximal oxidation values of PC and P700 and maximal reduction of Fed, as determined with the NIRMAX protocol, of which a 3-s illumination with actinic light is shown here (see Supporting Information Fig. S9 for the full experiment), including a multiple turnover pulse after 200 ms (indicated by the red triangle in the WT panel). Averaged traces from six (WT), five (ΔFed4), four (ΔFed9), or three (ΔFed3, ΔFed6, ΔFed789, ΔFed10, and ΔFed11) biological replicates are shown, with SD as the shadowed area. NIR, near-infrared.

PCC of Flv1/3 interactions with Chl increased to 0.41 ± 0.01 (Figs 5e, S16a) and that of Flv2/4 interactions to 0.28 ± 0.01 (Figs 5f, S16b). Supplementing nigericin with the potassium-specific ionophore valinomycin (40 µM) further increased the PCC of Flv2/4 interactions with Chl fluorescence to 0.39 ± 0.01 (Figs 5F, S16d). The addition of DCMU, which blocks electron transport from PSII and thus partly inhibits *pmf* generation (Fig. S16), also increased the PCC of both Flv1/3 and Flv2/4 interaction signals with Chl fluorescence (Fig. 5e,f), although results were visually less clear than with the uncouplers (Fig. S17). Immunoblotting analysis showed that CCCP significantly decreased the amount of Flv1 in the soluble fraction, with a nonsignificant increase in the membrane fraction (Fig. S18a). The CCCP also slightly decreased the Flv2 amount in the soluble fraction, while Flv4 remained exclusively in the membrane fraction (Fig. S18a). Contamination of the membrane fraction by soluble proteins, indicated by the presence of the large Rubisco subunit (Fig. S18b), resulted in variation between replicates, reducing the significance of observed effects. Computational modelling of Flv1-VN + Flv3-VC complexes predicted that the Venus fusions do not interfere with the formation of functional FDP heterooligomers (Fig. 5g).

These results suggest that a more acidic pH allows FDP heterooligomers to associate with the thylakoid membrane, likely enabling rapid activation of the Mehler-like reaction, for example, during dark-to-light transitions. Conversely, increased *pmf* and cytosolic alkalisation cause disassociation from the thylakoid membrane. Indeed, 15 µM CCCP, which dissipates *c.* 30% of the *pmf* (Fig. S13), increased the peak O_2 photoreduction rate relative to maximum O_2 evolution from 39 to 69%, and 30 µM CCCP to 87% (Fig. S19a). No O_2 photoreduction was detected in the ΔFlv3 mutant under these conditions (Fig. S19b), indicating that the effect is FDP dependent. Since CCCP also inhibits photosynthesis, interpretation of these MIMS results is complex. To address this, we measured the O_2 photoreduction rate in the presence of 20 µM nigericin, which had a minor effect on O_2

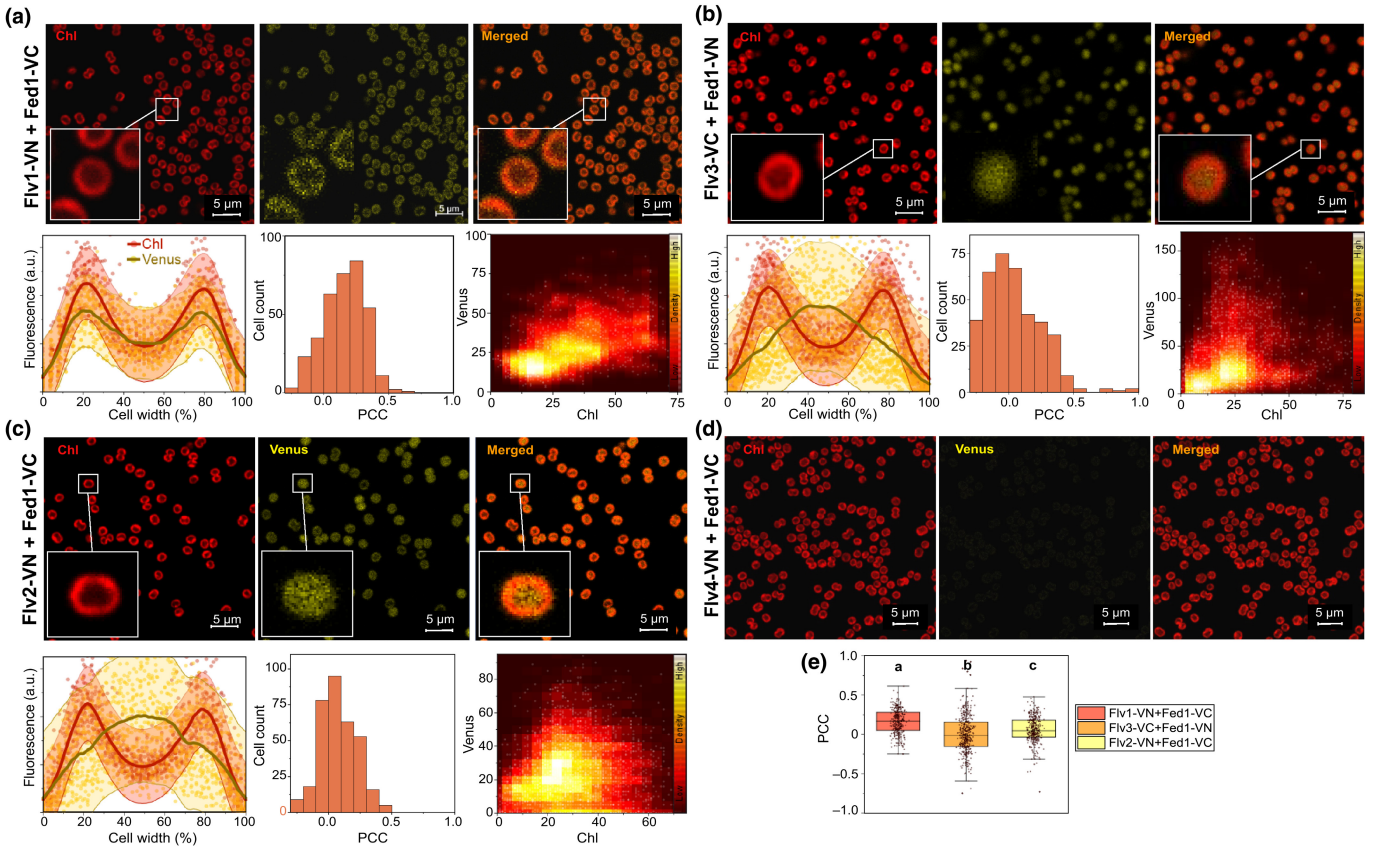

Fig. 4 Interactions between ferredoxin 1 (Fed1) and flavodiiron proteins (FDPs) in *Synechocystis* in bimolecular fluorescence complementation (BiFC) tests. Representative confocal micrographs from three independent experiments are presented, showing Chl autofluorescence emanating from the thylakoid membranes in the left panel, fluorescence from re-assembled Venus I152L fluorescent proteins in the middle, and overlaid Chl and Venus fluorescence on the right panel. (a) Flv1-VN + Fed1-VC, (b) Flv3-VC + Fed1-VN, (c) Flv2-VN + Fed1-VC, and (d) Flv4-VN + Fed1-VC. The inlets show zoomed-in views of a single cell. For quantification of the subcellular localisations of the interacting fusion protein pairs, the co-localisation of Chl (red) and Venus (yellow) fluorescence is also presented with fluorescence intensities over 5-pixel-wide cross-sections of 30 cells (with width normalised to 100%) shown as a scatter plot. Red and gold lines show moving regression curves produced by locally weighted scatter plot smoothing (LOWESS) with 120 points of window. 95% confidence intervals are shown as the pale colour shadows. The histogram shows the distribution of the Pearson correlation coefficient (PCC) for Chl and Venus fluorescence co-localisation in all cells from three micrographs from individual replicates. A PCC of 1 indicates perfect co-localisation and a PCC of 0 no co-localisation. The cytofluorogram shows co-localised Chl and Venus fluorescence intensities as a scatter plot. (e) Comparison of PCC values for Chl and Venus fluorescence co-localisation between Flv1-VN + Fed1-VC, Flv3-VC + Fed1-VN, and Flv2-VN + Fed1-VC cultures. Box plots with median ± SD and individual data points as dots are shown. Statistical significance is indicated by lowercase letters according to one-way ANOVA and Tukey's *post hoc* tests for comparisons of means ($P < 0.05$).

evolution (Fig. S20b). Nigericin caused a significant increase in the maximal O_2 photoreduction rate (normalised to maximal O_2 gross evolution rate) in WT cells (Fig. 6), while no nigericin-induced O_2 photoreduction was detected in the ΔFlv3 mutant (Fig. S20c). Addition of nigericin also did not affect the redox kinetics of Fed (Fig. S20d).

The ΔD1D2 mutant, lacking NdhD1 and NdhD2 subunits of the NDH-1 complex, maintains a high O_2 photoreduction rate (up to 80–90% of gross O_2 evolution; Nikkanen *et al.*, 2020). The AY and AO fluorescence measurements showed delayed cytosolic alkalisation in this strain (Fig. S21), suggesting that a more acidic cytosol allows FDP heterooligomers to remain at the thylakoid membrane, sustaining high O_2 photoreduction. Inhibition of respiratory terminal oxidases by KCN also delayed cytosolic alkalisation (Fig. S21) and increased light-dependent O_2 uptake (Fig. S22a), likely from photorespiration rather than the Mehler-like reaction, as shown by CO_2 production in the ΔFlv3 D1D2 mutant (Fig. S22b). KCN-treated cells had slightly higher cytosolic pH (Fig. S21a) and significantly higher *pmf* (Fig. S22c). In line with this, KCN decreased Flv2/4 interactions with the thylakoid membrane (Fig. S23c,d), while no effect was observed on Flv1/3 interactions (Fig. S24c,d).

We tested the impact of cellular thiol redox state on Flv1/3 or Flv2/4 localisation by adding 2 mM dithiothreitol (DTT; reducing) or 100 μM cupric chloride ($CuCl_2$; oxidising). DTT did not affect FDP heterooligomer localisation, while $CuCl_2$ slightly decreased their thylakoid association (Figs S23, S24). DTT had minimal effect on *pmf*, O_2 evolution, or light-induced O_2 uptake, but increased dark respiration. $CuCl_2$ partially inhibited O_2 evolution and slightly elevated *pmf* (Fig. S22). Cation concentration changes in the medium did not alter Flv1/3 or Flv2/4 interactions (Fig. S25).

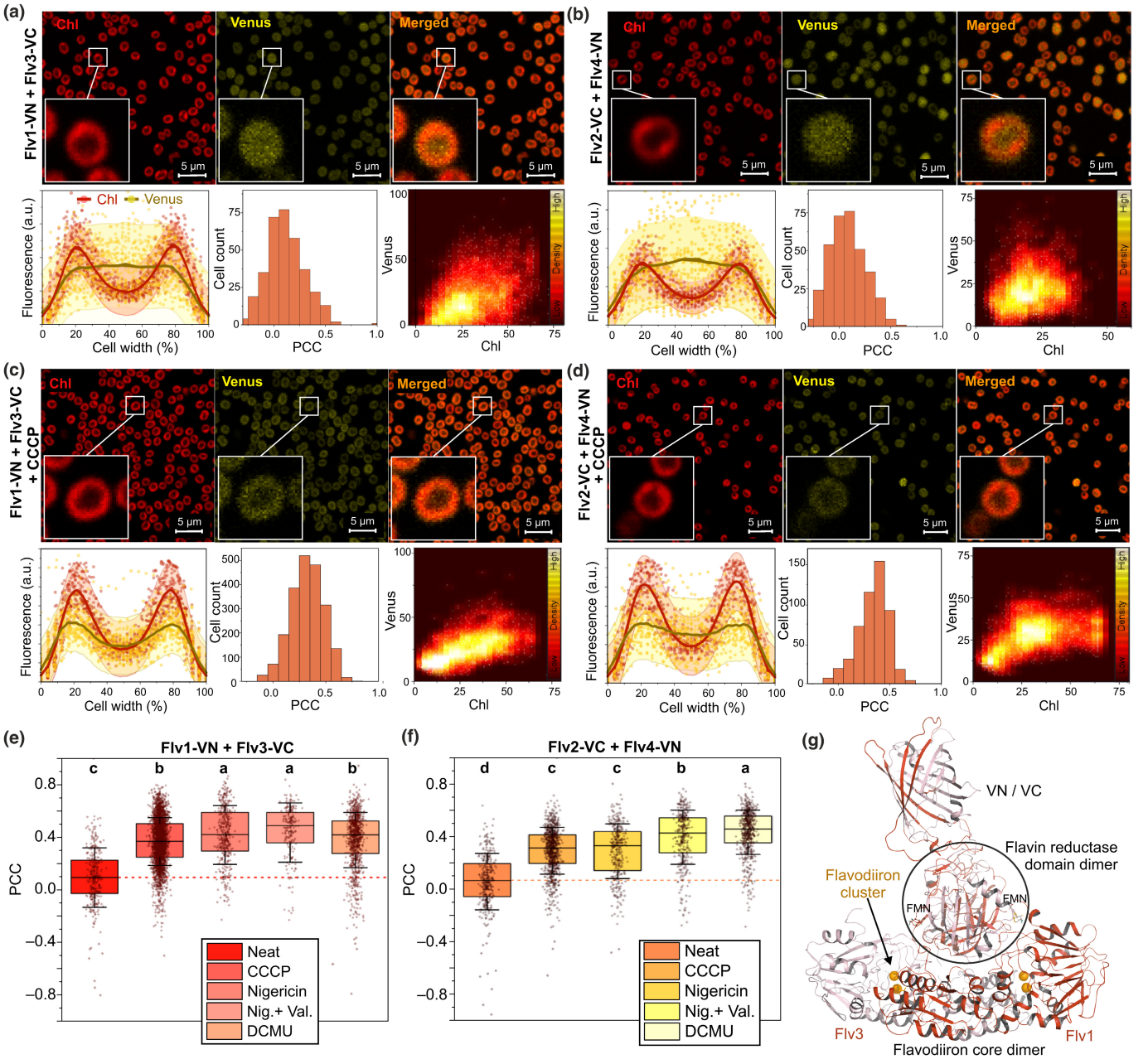

Fig. 5 Subcellular localisations of Flv1/3 and Flv2/4 interactions in *Synechocystis* in bimolecular fluorescence complementation (BiFC) tests. (a) BiFC tests between Flv1-VN and Flv3-VC. (b) BiFC tests between Flv2-VC and Flv4-VN. (c) BiFC tests between Flv1-VN and Flv3-VC with 30 µM carbonyl cyanide m-chlorophenylhydrazone (CCCP) added in the medium. (d) BiFC tests between Flv2-VC and Flv4-VN with 30 µM CCCP added in the medium. Upper panels show representative confocal micrographs from the Chl and Venus fluorescence channels as well as a merged image. The inlets show zoomed-in views of a single cell. For quantification of the subcellular localisations of the interacting fusion protein pairs, the co-localisation of Chl (red) and Venus (yellow) fluorescence is also presented with fluorescence intensities over 5-pixel-wide cross-sections of 48 (a), 50 (b), 39 (c), and 44 (d) cells (with width normalised to 100%) shown as a scatter plot. Red and gold lines show moving regression curves produced by locally weighted scatter plot smoothing (LOWESS) with 120 points of window. Ninety-five per cent confidence intervals are shown as pale colour shadows. The histogram shows the distribution of the Pearson correlation coefficient (PCC) for Chl and Venus fluorescence co-localisation in all cells from three micrographs from individual replicates. A PCC of 1 indicates perfect co-localisation and a PCC of 0 no co-localisation. The cytofluorogram shows co-localised Chl and Venus fluorescence intensities as a scatter plot. (e, f) Comparison of PCC values for Chl and Venus fluorescence co-localisation between untreated (Neat) Flv1-VN + Flv3-VC (e) and Flv2-VC + Flv4-VN (f) cultures and cultures treated with 30 µM CCCP, 20 mM nigericin, 20 mM nigericin (Nig.) and 40 µM valinomycin (Val.), or 20 µM DCMU. Box plots with median ± SD and individual data points as dots are shown. Statistical significance is indicated by lowercase letters according to one-way ANOVA and Tukey's *post hoc* tests for comparisons of means ($P < 0.05$). The dotted lines indicate the medians of the neat experiments. (g) Predicted structure of an Flv1-VN + Flv3-VC interaction complex.

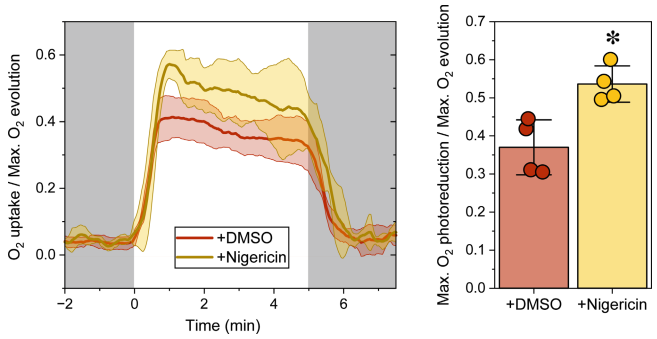

Fig. 6 Effect of nigericin on the *Synechocystis* O_2 photoreduction rate. O_2 exchange in wild-type (WT) cells grown under 3% [CO_2] at 50 μmol photons m^{-2} s^{-1} and at pH 7.5 was measured by membrane-inlet mass spectrometry (MIMS) during dark and 5 min of illumination at 500 μmol photons m^{-2} s^{-1}. Cells were measured either in the presence of 4 μl DMSO solvent as control or with 20 μM nigericin (in 4 μl DMSO). The traces are shown as O_2 uptake rate/maximal O_2 gross evolution rate, and are averaged from four biological replicates ±SD. The right-hand panel shows the mean ratios between maximal light-induced O_2 uptake and maximal gross O_2 evolution with and without 20 μM nigericin ±SD with individual datapoints shown as circles. Statistical significance of the difference was tested by a two-sample *t*-test and is indicated: *, $P = 0.0113$.

Subcellular localisation of Flv1 and Flv3 self-interactions

Flv1 showed self-interactions primarily on the thylakoids (Fig. S26a), suggesting either homooligomerisation or involvement in higher-order heterooligomers. Flv3 self-interactions varied, with most cells showing weak interaction signals on the thylakoids, while a subpopulation exhibited stronger signals in the cytosol (Fig. S26b). High cation concentration and CCCP slightly decreased cytosolic Flv3 self-interactions (Fig. S27).

No interaction was detected between Flv3-VN and Flv2-VC (Fig. S26c), despite strong expression of both fusion proteins (Fig. S8), supporting the inability of Flv2 and Flv3 to form heterooligomers *in vivo* (Mustila *et al.*, 2016), as well as providing a negative control for the observed interactions.

Surface charge modelling supports pH-dependent association of FDP heterooligomers with the thylakoid membrane

We examined the molecular mechanism underlying the ΔpH-dependent association of FDP heterooligomers with the thylakoid membrane. At low *pmf*, the low pH on the cytosolic side of the thylakoid membrane may protonate acidic residues in proteins, making their surface charge more positive, and promoting electrostatic interactions with negatively charged membrane lipids or other proteins in the membrane (Johnson & Cornell, 1999; Mulgrew-Nesbitt *et al.*, 2006). To test this hypothesis, we modelled the electrostatic surface potentials of FDP monomers and oligomers at physiologically relevant pH values. In cyanobacteria, cytosolic pH ranges from 7 in dark or low light to 8.5 under strong illumination, depending on extracellular pH (Coleman & Colman, 1981; Mangan *et al.*, 2016).

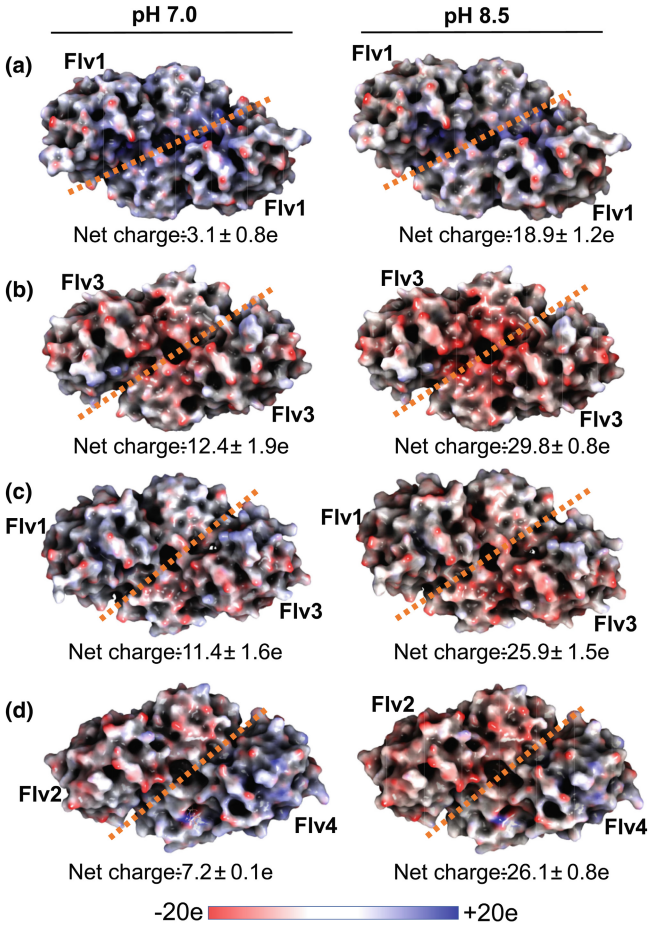

Fig. 7 *In silico* analysis of the electrostatic surface of flavodiiron protein (FDP) oligomers at different pH. (a) Flv1/Flv1 homodimer, (b) Flv3/Flv3 homodimer, (c) Flv1/Flv3 heterodimer, and (d) Flv2/Flv4 heterodimer. Surface charges are colour-coded, with red representing negative charge, blue positive charge, and white neutral regions. Net charges with SD are shown. The left and right panels show charges at pH 7.0 and pH 8.5, respectively. Since the relative orientation of the C-terminal flavin reductase domain could not be modelled reliably, only the β-lactamase-like and flavodoxin-like domains are shown. The orange line indicates the symmetry axis between monomers.

Our analysis predicted that at pH 7.0, Flv1 and Flv3 core monomers have net surface charges of −3.0 ± 0.2e and −11.5 ± 0.6e, respectively. At a more alkaline pH of 8.5, these charges become more negative, with Flv1 at −9.3 ± 0.6e and Flv3 at −18.5 ± 1.1e (Fig. S28a,c). Flv1 core homodimers exhibit a small negative net charge of −3.1 ± 0.8e at neutral pH, with positively charged patches that remain at alkaline pH, when the net charge becomes −18.9 ± 1.2e. These patches may facilitate membrane interactions, albeit with lower affinity at alkaline pH (Fig. 7a). By contrast, Flv3 core homodimers have a negative net charge of −12.4 ± 1.9e at pH 7.0, which becomes more negative (−29.8 ± 0.8e) at pH 8.5 (Fig. 7b). Flv1/3 core heterooligomers carry a net charge of −11.4 ± 1.6e, with positively charged patches that likely permit interaction with negatively charged membrane lipids. However, at pH 8.5, the Flv1/3

heterooligomer becomes highly negatively charged (−25.9 ± 1.5e), reducing its ability to interact with the membrane due to electrostatic repulsion (Fig. 7c).

Monomeric Flv2 and Flv4, in turn, carry contrasting net charges. Flv2 has a highly negative net charge at both pH 7.0 and 8.5 (−16.2 ± 0.4e and −24.2 ± 0.8e), while Flv4 has a positive charge (+5.8 ± 0.1e) at pH 7.0 and a slightly negative charge at pH 8.5 (−2.2 ± 0.2e) with large positive patches (Fig. S28b,d). The Flv2/Flv4 heterooligomer has a mostly negative charge of −7.2 ± 0.1e at pH 7.0. At pH 8.5, its interaction with negatively charged membrane surfaces is hindered due to a highly negative net charge of −26.1 ± 0.8e (Fig. 7d).

Discussion

Light-dependent reduction of O_2 to H_2O by FDPs, known as the Mehler-like reaction, constitutes a vital, strictly regulated outlet for excessive electrons in the PETC during fluctuations in light intensity (Allahverdiyeva *et al.*, 2013; Alboresi *et al.*, 2019; Nikkanen *et al.*, 2021b). As photosynthetic microorganisms are increasingly employed as green cell factories for sustainable bioproduction, understanding the regulatory mechanisms of photosynthesis is crucial for optimising the photon-to-product conversion efficiency (Nikkanen *et al.*, 2021a; Hubáček *et al.*, 2024). Flavodiiron proteins form various homo- and heterooligomeric conformations, but heterooligomers consisting of Flv1 and Flv3 as well as Flv2 and Flv4 are required for the Mehler-like reaction under air-level [CO_2] in *Synechocystis* (Mustila *et al.*, 2016; Santana-Sanchez *et al.*, 2019). Several key aspects of this essential regulatory mechanism of photosynthesis, however, have remained unclear. (1) What is the electron donor to different FDP homo- and heterooligomeric conformations? (2) What kind of oligomers can FDPs form and how do they localise within the cell? (3) How is the activity of the Mehler-like reaction controlled? Using a BiFC system to visualise protein–protein interactions, biochemical and biophysical characterisation of photosynthetic electron transport in *Synechocystis* mutants, and *in silico* surface charge modelling allowed us to address these questions in the present study.

Previous studies have shown that NAD(P)H can donate electrons to recombinant Flv1 or Flv3 (Vicente *et al.*, 2002; Brown *et al.*, 2019) as well as to Flv4 (Shimakawa *et al.*, 2015) *in vitro*. However, as also pointed out by Shimakawa *et al.* (2022), the observed *in vitro* rates are too low to explain the *in vivo* rates of O_2 photoreduction. The maximal NAD(P)H-dependent O_2 reduction rate for Flv1 or Flv3 *in vitro* was *c.* 30 μmol O_2 mg^{-1} Flv1 min^{-1} (Brown *et al.*, 2019), whereas the maximal *in vivo* O_2 photoreduction rates in WT *Synechocystis* under strong illumination in air-level [CO_2] are *c.* 100 μmol O_2 mg^{-1} Chl h^{-1} (Santana-Sanchez *et al.*, 2019). In high [CO_2] conditions, similar rates are maintained even though Flv2 and Flv4 are not expressed (Santana-Sanchez *et al.*, 2019) and Flv1 and Flv3 are less abundant than in air-level [CO_2] (Zhang *et al.*, 2009). Based on recent absolute quantification of Flv1 proteins (1100–1400 copies per cell) and Chl molecules (*c.* 1.54E+07 copies per cell; Jackson *et al.*, 2023), the *in vivo* rate converts to *c.* 270 μmol O_2 mg^{-1} Flv1 min^{-1}, which is ninefold higher than the *in vitro* rate reported for Flv1 (Brown *et al.*, 2019). The NADH-dependent O_2 reduction rate for Flv4 *in vitro* was much lower at *c.* 0.29 μmol O_2 mg^{-1} Flv4 min^{-1} (Shimakawa *et al.*, 2015).

Moreover, Flv1 and Flv3 monomers or homooligomers cannot catalyse the Mehler-like reaction *in vivo* (Mustila *et al.*, 2016). In this study, we found that severe impairment of light-induced $NADP^+$ reduction in the ΔFNR_L mutant did not significantly affect the O_2 photoreduction activity of FDPs or the ability to rapidly re-oxidise Fed or P700 under strong illumination (Fig. 1). The slight decrease in O_2 photoreduction observed in ΔFNR_L under air-level [CO_2] was due to diminished Flv2 content. However, under elevated [CO_2], where the *flv4-2* operon is not expressed (Zhang *et al.*, 2009), the difference in O_2 photoreduction between WT and ΔFNR_L was abolished (Fig. 1). The slight increase in Flv1 and Flv3 abundance in ΔFNR_S and (insignificantly) in ΔFNR_L (Fig. 1e) might reflect a compensatory response to the limitation of FNR as an electron acceptor from Fed, creating more reduction pressure on the Fed pool and potentially triggering an upregulatory signal to increase the transcription of *flv1* and *flv3*. Moreover, as FNR_S likely feeds electrons to NDH-1 catalysing CET (Miller *et al.*, 2022), and functional redundancy exists between Flv1/Flv3 and NDH-1 in maintaining efficient PSI oxidation (Nikkanen *et al.*, 2020; Storti *et al.*, 2020), the upregulation of Flv1 and Flv3 may constitute compensation for impaired CET in ΔFNR_S.

Although NADPH is generated in the dark via the oxidative pentose phosphate pathway and FDPs can use NADH for O_2 reduction *in vitro* (Shimakawa *et al.*, 2015; Brown *et al.*, 2019), it is unlikely that light-independent NADPH or NADH production powers the light-dependent Mehler-like reaction in ΔFNR_L. Increased dark respiration in ΔFNR_L (Fig. S4c) was possibly due to more abundant FNR_S, shuttling electrons from NADPH to NDH-1 via Fed in a respiratory/cyclic pathway (Miller *et al.*, 2022).

Together with previous reports on Fed and NADPH redox kinetics in FDP mutants (Nikkanen *et al.*, 2020; Sétif *et al.*, 2020), our results suggest that neither NADPH nor FNR is the main electron donor for the Mehler-like reaction catalysed by Flv1/3 and Flv2/4 heterooligomers. This poses the question of the C-terminal domain's physiological role, which could involve Fed binding or electron transfer from a reduced flavodoxin domain to reduce $NADP^+$ (Sétif *et al.*, 2020). This could protect the catalytic diiron centre of the enzyme by relieving its overreduction, for example in low [O_2] conditions (Sétif *et al.*, 2020). The C-terminal domain may also be involved in the unknown physiological function of FDP homooligomers.

We observed a protein–protein interaction between FNR_L and Flv3, localised to the thylakoid membrane (Fig. 2). The MIMS results suggest that FNR_L does not function as an electron donor to Flv1/3 in the Mehler-like reaction. Instead, FNR_L may interact with Flv3 homooligomers to perform an unknown function on thylakoids or possibly associated with the phycobilisomes, to which FNR binds (Liu *et al.*, 2019). While Flv3 homooligomers do not catalyse the Mehler-like reaction, their abundance (four- to sixfold more than Flv1; Jackson *et al.*, 2023) and partial rescue

of the ΔFlv1 mutant phenotype in fluctuating light by overexpressing Flv3 (in ΔFlv1 background, Mustila *et al.*, 2016) suggest a non-Mehler-like photoprotective role. Considering the *in vitro* NAD(P)H donation to recombinant Flv3 and the NAD(P)H:flavin oxidoreductase-like domain in FDPs, *in vivo* NAD(P)H may donate electrons to Flv3 homooligomers via FNR_L interaction.

While false positives in BiFC due to protein proximity cannot be ruled out, the strong Venus fluorescence signal and the near absence of interaction signal between Flv1 and FNR_L and comparable abundance of fusion proteins (Fig. S6) suggest that this is unlikely. The BiFC negative results should nonetheless also be interpreted with caution. Unfavourable structural orientation of the Venus fragments in the interaction complex, steric hindrance, or improper folding of the fusion proteins may prevent reassembly of a functional fluorophore (Kudla & Bock, 2016). In the current study, to minimise topological constraints and steric hindrance, we introduced a flexible linker sequence between the proteins of interest and the Venus fragments. Computational modelling (Fig. 5g) supports the BiFC results, indicating that FDP-VN/C monomers from different oligomers would not interact, and any endogenous FDP interactions are negligible due to the higher abundance of fusion proteins. This is particularly relevant for Flv2 and Flv4, which are not expressed under high $[CO_2]$, as in this study.

Recent *in vivo* studies indicate that Fed is the likely electron donor to Flv1/3 (Nikkanen *et al.*, 2020; Sétif *et al.*, 2020), and a recombinant class A FDP from the protozoan *Entamoeba histolytica* can oxidise Fed *in vitro* (Cabeza *et al.*, 2015). Out of the low-abundance Fed isoforms (Fed2-Fed11), only Fed2 is essential for photoautotrophic growth in *Synechocystis* (Cassier-Chauvat & Chauvat, 2014), although it functions in low-iron response instead of photosynthetic electron transfer (Schorsch *et al.*, 2018), making it an unlikely primary donor to FDPs. Isoforms Fed7, 8, and 9 are associated with stress response in cooperation with the thioredoxin system (Marteyn *et al.*, 2009; Mustila *et al.*, 2014), and Fed9 supports photomixotrophic growth, likely via electrons from pyruvate:ferredoxin oxidoreductase (Wang *et al.*, 2022). These bacterial-type, low-abundance Feds are therefore unlikely to provide the main electron source for the light-induced Mehler-like reaction, despite the two-hybrid interaction reported between Fed9 and Flv3 (Cassier-Chauvat & Chauvat, 2014). Accordingly, we detected no statistically significant impairment of the Mehler-like reaction in mutant strains lacking Fed2-Fed11 (Figs 3, S7, S8). We showed that Fed1 interacts *in vivo* with Flv1, Flv3, and Flv2 (Fig. 4). Although minor or redundant roles, or even roles as electron acceptors from FDPs for low-abundance Feds, such as Fed9 cannot be entirely excluded, and *in vitro* evidence of Fed-dependent O_2 reduction by cyanobacterial FDP heterooligomers is still lacking, these results strongly suggest that Fed1 is the main electron donor to FDP heterooligomers. Interestingly, no interaction was detected between Fed1 and Flv4 (Fig. 4). This suggests that Fed1 docking and electron transfer from Fed1 to Flv2/4 heterooligomers may occur via Flv2 or, as the BiFC experiments were performed under elevated $[CO_2]$ conditions, that Flv2 or another cofactor that is only present under low $[CO_2]$ is required for Fed1-Flv4 interactions to occur.

Flv1/Fed1 and Flv3/Fed1 interactions showed distinct subcellular localisations: Flv1 interacted with Fed1 at the thylakoids, while Flv3 mostly localised in the cytosol (Fig. 4). Due to high fusion protein expression (Fig. S6), the Flv3 pool in Fed1-VN + Flv3-VC cells was much larger than Flv1, likely causing a large proportion of Flv3-VC proteins to form homooligomers. The opposite is true in Fed1-VC + Flv1-VN cells. This would suggest that Flv1 homooligomers consistently localised to the thylakoids and Flv3 homooligomers to the cytosol. However, in a majority of cells, Flv3 self-interactions (Fig. S25b) and Flv3-FNR_L interactions (Fig. 2a) localised to the thylakoids, and the thylakoidal Flv3 self-interaction signals intensified in high concentrations of Ca^{2+} and Mg^{2+} cations (Fig. S26). These results suggest that the formation of Flv3 homooligomers and/or their association with the thylakoids and FNR may be controlled by the physiological state of the cell, while Flv1 homooligomers consistently associate with the thylakoid membrane. These observations were supported by modelling of surface charges, showing that Flv1 homooligomers' low net negative charge with large positively charged patches enabled thylakoid binding, whereas Flv3's highly negative charge reduced its thylakoid affinity (Barber, 1982; Fig. 7). Further studies are required to elucidate the physiological roles of FDP homooligomers.

Different cyanobacterial species show variability in FDP oligomer formation and its physiological significance. In *Anabaena* sp. PCC 7120, vegetative cell-specific Flv1A and Flv3A likely form heterooligomers similar to their *Synechocystis* orthologues. However, Flv3A alone appears to contribute to the Mehler-like reaction and PSI photoprotection through an unknown mechanism requiring Flv2 and Flv4 (Santana-Sánchez *et al.*, 2023). This suggests possible functional oligomers consisting of Flv3 and Flv2/4 or Flv3 homooligomers interacting with Flv2/4 heterooligomers in vegetative cells. In line with a previous biochemical analysis, we detected no Flv3-Flv2 interaction in *Synechocystis* (Fig. S25c), but such interactions in *Anabaena* or other species remain to be studied.

The addition of the *pmf*-uncoupling ionophore CCCP or the K^+/H^+ exchanger nigericin enhanced thylakoid localisation of Flv1/3 and to a lesser extent Flv2/4 interactions (Figs 5, S15), and increased the maximal light-induced O_2 uptake relative to O_2 evolution (Figs 6, S19). The transience of O_2 photoreduction suggests reversible post-translational regulation of Flv1/3 activity, and several putative mechanisms, such as a redox regulation by the thioredoxin system or phosphorylation and dephosphorylation, have been proposed (Alboresi *et al.*, 2019; Nikkanen *et al.*, 2021b; Beraldo *et al.*, 2024). Our findings in the current study suggest that FDP heterooligomers are amphitropic: cytosolic pH regulates their activity by determining whether they associate with the thylakoid membrane. As up to 75% of *pmf* generation during dark-to-light transitions in *Synechocystis* depends on FDP-catalysed O_2 photoreduction (Nikkanen *et al.*, 2020), we propose a feedback loop: in darkness or low light, low *pmf* and near-neutral cytosolic pH enable FDP heterooligomers to associate with the thylakoid membrane, catalysing

rapid and strong O_2 photoreduction (Fig. 8a), when CO_2 fixation has not been yet fully activated and photosynthetic control at Cyt b_6f is relaxed. This elevates *pmf* by proton consumption on the cytosolic side and oxidation of Fed1, supporting higher electron transport in the PETC. The resulting alkaline cytosolic pH then causes Flv1/3 heterooligomers to disassociate from the thylakoids, decreasing O_2 reduction activity after an initial peak (Fig. 8b). This aligns with previous findings where O_2 photoreduction peaks after *c.* 20–30 s of illumination, which is also when a steady-state level of *pmf* is reached in WT cells (Nikkanen *et al.*, 2020). After 30 s, the rate of O_2 photoreduction declines, especially in low [CO_2] or alkaline pH conditions where Flv2/4 are not expressed (Santana-Sanchez *et al.*, 2019).

Thylakoid association of FDP heterooligomers enhances their proximity to PSI-reduced Fed1, increasing the likelihood of interactions and amplifying the Mehler-like reaction. Similarly, the cyanobacterial bidirectional (NiFe) hydrogenase, when dynamically associating with the thylakoid membrane or being fused to PSI, exhibits higher photohydrogen production (Burroughs *et al.*, 2014; Appel *et al.*, 2020). This spatial proximity minimises diffusion limitations and facilitates efficient electron transfer. Likewise, thylakoid-associated FNR shows higher activity than its soluble form due to its enhanced proximity to reduced Fed (Carrillo & Vallejos, 1982; Forti & Bracale, 1984).

It has been reported previously that Flv2 and Flv4 are in the thylakoid fraction when *Synechocystis* proteins are extracted in a buffer containing Mg^{2+} and Ca^{2+} but shift to the soluble fraction in cation-depleted buffers (Zhang *et al.*, 2012). During dark-to-light transitions, *pmf* generation was delayed in low cation media (Fig. S13), likely due to the impairment of cation channels or antiporters on the thylakoid membrane (Carraretto *et al.*, 2016), diminishing the initial $\Delta\psi$ component. However, we detected no differences in Flv2/4 localisation between low and high cation media (Fig. S24c–d). Moreover, increased thylakoid localisation of FDP heterooligomer interactions was induced by the addition of nigericin, which acts as an H^+/K^+ exchanger, specifically dissipating the proton gradient while maintaining membrane potential (Figs 5, S15). A slight further increase in Flv2/Flv4 but not in Flv1/Flv3 thylakoid localisation was induced by the addition of the potassium-specific ionophore valinomycin (Figs 5, S15). These results suggest that the loss of the ΔpH component of *pmf* specifically promotes Flv1/Flv3 thylakoid association, while Flv2/Flv4 localisation may also be affected by the ionic balance across the thylakoid membrane.

In plant chloroplasts, low stromal pH promotes FNR binding to its membrane anchor Tic62 (Benz *et al.*, 2009). It is necessary to investigate in future studies whether the FDP:Fed1 interactions observed herein are themselves pH dependent, and to elucidate the molecular mechanism of electron transfer from Fed1 to FDP heterooligomers.

In silico modelling revealed that the molecular mechanism underlying the reversible association of FDP heterooligomers with the thylakoid membrane depends on changes in net surface charges within a physiological pH range (Fig. 7). In neutral cytosolic pH, such as in dark- or low-light conditions, Flv1/3 and Flv2/4 heterooligomers maintain a low negative net charge with positive patches that enable interaction with membrane

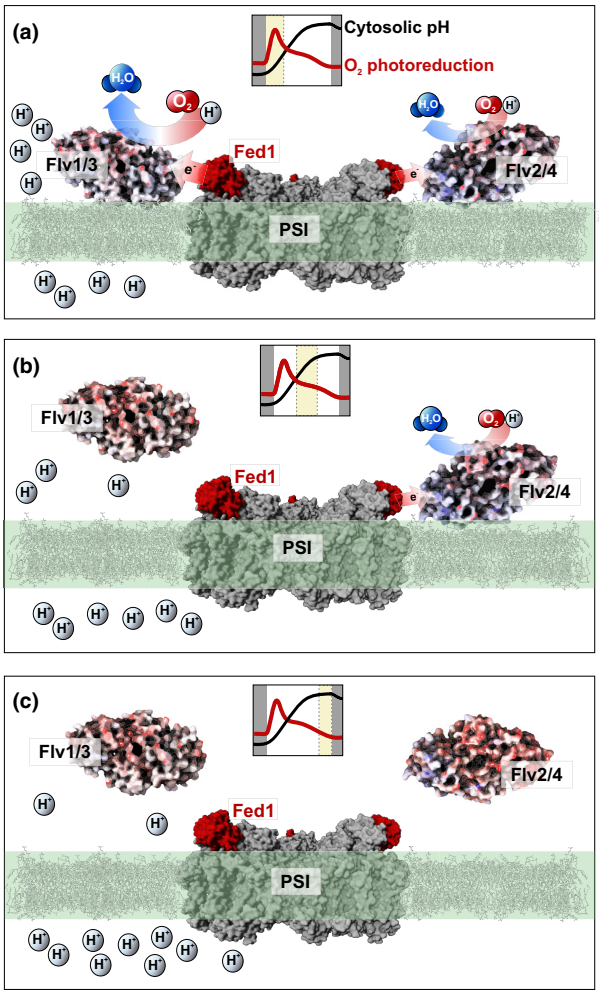

Fig. 8 Schematic model for pH-dependent association of flavodiiron protein (FDP) heterooligomers with the thylakoid membrane. (a) In dark or low light when *pmf* is low and cytosolic pH close to neutral, a more positive surface charge of FDP heterooligomers allows them to bind to the thylakoid membrane. This enables the rapid activation of FDPs upon illumination, catalysing a strong Mehler-like reaction using electrons from reduced ferredoxin 1 (Fed1). The process triggers swift *pmf* generation during dark-to-light or low-to-high light transitions in *Synechocystis* (Nikkanen *et al.*, 2020). (b) As *pmf* rises and the cytosol becomes increasingly alkaline, a self-regulatory feedback mechanism of FDPs is initiated. Flv1/3 heterooligomers are repelled from the membrane due to their surface charges becoming more negative. This inhibits Flv1/3 activity and results in the decline of the O_2 photoreduction rate. Due to the positive charge of Flv4, however, Flv2/4 heterooligomers still maintain affinity to the thylakoid membrane, catalysing residual O_2 photoreduction. (c) When the cytosol becomes highly alkaline upon full activation of CO_2 fixation, both FDP heterooligomers disassociate from the thylakoids, strongly inhibiting (now unnecessary) O_2 photoreduction activity. Trimeric Photosystem I (PSI) structure with bound Fed is based on Li *et al.* (2022). The small inlets within each panel represent typical kinetics of O_2 photoreduction in red, and alkalisation of the cytosol (Supporting information Fig. S14b) in black during a dark-to-light transition. The yellow rectangles indicate the phase depicted in the panel.

lipids or positively charged membrane proteins. By contrast, at higher pH mimicking the alkalisation of the cytosol upon strong illumination, the net charges of FDP heterooligomers become highly negative, repelling them from the membrane. As the cytosol gradually gets more alkaline under illumination (Fig. S21), the positive net charge of Flv4 (Fig. S28d) may allow Flv2/4 heterooligomers to remain bound to the membrane longer than Flv1/3 heterooligomers (Fig. 8b,c). This could explain the distinct kinetics of Flv1/3 and Flv2/4-mediated O_2 photoreduction, where Flv1/3 catalyses a strong but transient reaction, and Flv2/4 a more sustained O_2 photoreduction further into dark–light transitions (Santana-Sanchez *et al.*, 2019).

It is worth pointing out that a decreased FDP activity in steady-state highlights, as proposed by our model (Fig. 8c), does not contradict *in vivo* findings. Although *pmf* generation occurs rapidly within milliseconds after the onset of high irradiance (Joliot & Joliot, 2008), alkalisation of the cytosol, resulting in the release of FDP heterooligomers from the membrane, does not happen instantly, as shown by the AO fluorescence measurements (Fig. S21). The highest O_2 photoreduction rates occur within the first minute of high-light transition, coinciding well with the lag in alkalisation of the cytosol. When full alkalisation is reached, FDP activity declines, depending on conditions and genotype, but typically to *c.* 25 μmol O_2 mg^{-1} Chl h^{-1} after 5 min of illumination at 500 μmol photons m^{-2} s^{-1} (Hubáček *et al.*, 2024). Rather than being necessary for photoprotection in high light, Flv1/3 heterooligomers are crucial during transitions to high light (i.e. light fluctuations). Accordingly, mutants lacking Flv1/3 cannot grow under fluctuating light conditions but grow as well as WT under continuous high light (Allahverdiyeva *et al.*, 2013).

The proposed pH-dependent regulatory mechanism of FDP activity may also indirectly control the induction of the carbon concentrating mechanism (CCM), as at least in algae, CCM induction was recently shown to depend on *pmf* generation by FDPs and CET (Burlacot *et al.*, 2022). Our recent results with *Anabaena* sp. PCC 7120 suggest that a similar dependency may also exist in cyanobacteria (Santana-Sánchez *et al.*, 2023).

In conclusion, the present study elucidates the regulation of the Mehler-like reaction and advances our understanding of how photoprotective mechanisms are orchestrated in dynamic, natural light environments. Our findings support Fed1 as the primary electron donor to both Flv1/3 and Flv2/4 heterooligomers. Furthermore, we demonstrated that the activity of the Mehler-like reaction is regulated by reversible association with the thylakoid membrane via pH-dependent changes in electrostatic surface charges of FDP heterooligomers. We propose a model of a self-regulatory feedback mechanism that controls the activity of the Mehler-like reaction. Our model posits that the Mehler-like reaction, by being crucial for the generation of *pmf* upon increases in light intensity, promotes its own inactivation by pH-dependent disassociation from the thylakoid membrane. This ensures that the Mehler-like reaction is downregulated to not waste energy when a release valve for excessive electrons in the PETC is not needed. By shedding light on the intricate mechanisms that optimise photosynthetic efficiency, our study provides a foundation for rationally directing electron flux towards desired reactions in photosynthesis-based biotechnological applications.

Acknowledgements

We thank Pauli Kallio for kindly providing plasmids for modular cloning and for helpful discussions, Laura Wey for valuable discussions, and Anniina Lepistö, Janette Vähäsarja, Sofia Westerlund, Ville Käpylä, Mahfuzur Rahman, and Linda Nevala for technical assistance. Biophysical experiments were performed within the PHOTOSYN infrastructure at the University of Turku, and confocal microscopy at the Cell Imaging and Cytometry Core, Turku Bioscience Centre, with the support of Biocenter Finland. We also thank the bioinformatics (JV Lehtonen), translational activities, and structural biology FINStruct infrastructure support from Biocenter Finland and CSC IT Center for Science for computational infrastructure support at the Structural Bioinformatics Laboratory (SBL), Åbo Akademi University. Research was funded by Research Council of Finland projects 'Revisiting Photosynthesis' (no. 315119 to YA), 'Channelling photosynthesis' (no. 354876 to LN), the NordForsk Nordic Center of Excellence 'NordAqua' (no. 82845 to YA), the Novo Nordisk Fonden 'PhotoCat' (no. NNF20OC0064371 to YA), and the China Scholarship Council (CSC) (grant no. 201406320187 to YW).

Competing interests

None declared.

Author contributions

LN and YA conceived the idea, designed the experiments, interpreted the data, and finalised the article with contributions from all authors. LN performed most of the experiments, analysed the data, and wrote the initial draft. SV and TAS performed the computational modelling. AS-S and MH performed additional cloning, generation of BiFC strains, and MIMS. MH also performed some of the DUAL-KLAS-NIR and NAD(P)H fluorescence measurements. GK created tools for microscopy image analysis. YW and MB generated the Fed mutants. KG and YA provided resources.

ORCID

Yagut Allahverdiyeva https://orcid.org/0000-0002-9262-1757
Michal Hubáček https://orcid.org/0000-0001-6507-7840
Lauri Nikkanen https://orcid.org/0000-0002-7192-9322

Data availability

The data that support the findings of this study are openly available in the Figshare database at doi: 10.6084/m9.figshare.28594964.

References

Alboresi A, Storti M, Cendron L, Morosinotto T. 2019. Role and regulation of class-C flavodiiron proteins in photosynthetic organisms. *The Biochemical Journal* **476**: 2487–2498.

Allahverdiyeva Y, Ermakova M, Eisenhut M, Zhang P, Richaud P, Hagemann M, Cournac L, Aro E-M. 2011. Interplay between flavodiiron proteins and photorespiration in *Synechocystis* sp. PCC 6803. *Journal of Biological Chemistry* **286**: 24007–24014.

Allahverdiyeva Y, Mustila H, Ermakova M, Bersanini L, Richaud P, Ajlani G, Battchikova N, Cournac L, Aro E-M. 2013. Flavodiiron proteins Flv1 and Flv3 enable cyanobacterial growth and photosynthesis under fluctuating light. *Proceedings of the National Academy of Sciences, USA* **110**: 2013.

Appel J, Hueren V, Boehm M, Gutekunst K. 2020. Cyanobacterial *in vivo* solar hydrogen production using a photosystem I–hydrogenase (PsaD-HoxYH) fusion complex. *Nature Energy* **5**: 458–467.

Artz JH, Tokmina-Lukaszewska M, Mulder DW, Lubner CE, Gutekunst K, Appel J, Bothner B, Boehm M, King PW. 2020. The structure and reactivity of the HoxEFU complex from the cyanobacterium *Synechocystis* sp. PCC 6803. *Journal of Biological Chemistry* **295**: 9445–9454.

Barber J. 1982. Influence of surface charges on thylakoid structure and function. *Annual Review of Plant Physiology* **33**: 261–295.

Beckmann K, Messinger J, Badger MR, Wydrzynski T, Hillier W. 2009. On-line mass spectrometry: membrane inlet sampling. *Photosynthesis Research* **102**: 511–522.

Benz JP, Stengel A, Lintala M, Lee Y-H, Weber A, Philippar K, Guegel IL, Kaieda S, Ikegami T, Mulo P *et al.* 2009. Arabidopsis Tic62 and ferredoxin-NADP(H) oxidoreductase form light-regulated complexes that are integrated into the chloroplast redox poise. *Plant Cell* **21**: 3965–3983.

Beraldo C, Traverso E, Boschin M, Cendron L, Morosinotto T, Alboresi A. 2024. Physcomitrium patens flavodiiron proteins form heterotetrameric complexes. *The Journal of Biological Chemistry* **20**: 107643.

Berman HM. 2000. The protein data bank. *Nucleic Acids Research* **28**: 235–242.

Blomberg MRA, Ädelroth P. 2023. Reduction of nitric oxide to nitrous oxide in flavodiiron proteins: catalytic mechanism and plausible intermediates. *ACS Catalysis* **13**: 2025–2038.

Brown KA, Guo Z, Tokmina-Lukaszewska M, Scott LW, Lubner CE, Smolinski S, Mulder DW, Bothner B, King PW. 2019. The oxygen reduction reaction catalyzed by *Synechocystis* sp. PCC 6803 flavodiiron proteins. *Sustainable Energy & Fuels* **3**: 3191–3200.

Burlacot A, Dao O, Auroy P, Cuiné S, Li-Beisson Y, Peltier G. 2022. Alternative photosynthesis pathways drive the algal CO_2-concentrating mechanism. *Nature* **605**: 366–371.

Burlacot A, Richaud P, Gosset A, Li-Beisson Y, Peltier G. 2020. Algal photosynthesis converts nitric oxide into nitrous oxide. *Proceedings of the National Academy of Sciences, USA* **117**: 2704–2709.

Burroughs NJ, Boehm M, Eckert C, Mastroianni G, Spence EM, Yu J, Nixon PJ, Appel J, Mullineaux CW, Bryan SJ. 2014. Solar powered biohydrogen production requires specific localization of the hydrogenase. *Energy & Environmental Science* **7**: 3791–3800.

Cabeza MS, Guerrero SA, Iglesias AA, Arias DG. 2015. New enzymatic pathways for the reduction of reactive oxygen species in *Entamoeba histolytica*. *Biochimica et Biophysica Acta (BBA) - General Subjects* **1850**: 1233–1244.

Carraretto L, Teardo E, Checchetto V, Finazzi G, Uozumi N, Szabo I. 2016. Ion channels in plant bioenergetic organelles, chloroplasts and mitochondria: from molecular identification to function. *Molecular Plant* **9**: 371–395.

Carrillo N, Vallejos RH. 1982. Interaction of ferredoxin-NADP oxidoreductase with the thylakoid membrane. *Plant Physiology* **69**: 210–213.

Cassier-Chauvat C, Chauvat F. 2014. Function and regulation of ferredoxins in the Cyanobacterium, *Synechocystis* PCC6803: recent advances. *Life (Basel)* **4**: 666–680.

Chaux F, Burlacot A, Mekhalfi M, Auroy P, Blangy S, Richaud P, Peltier G. 2017. Flavodiiron proteins promote fast and transient O-2 Photoreduction in Chlamydomonas(1[OPEN]). *Plant Physiology* **174**: 1825–1836.

Coleman JR, Colman B. 1981. Inorganic carbon accumulation and photosynthesis in a blue-green alga as a function of external pH. *Plant Physiology* **67**: 917–921.

Folgosa F, Martins MC, Teixeira M. 2018. Diversity and complexity of flavodiiron NO/O_2 reductases. *FEMS Microbiology Letters* **365**: 1259.

Forti G, Bracale M. 1984. Ferredoxin ferredoxin NADP reductase interaction – catalytic differences between the soluble and thylakoid-bound complex. *FEBS Letters* **166**: 81–84.

Gerotto C, Alboresi A, Meneghesso A, Jokel M, Suorsa M, Aro E-M, Morosinotto T. 2016. Flavodiiron proteins act as safety valve for electrons in *Physcomitrella patens*. *Proceedings of the National Academy of Sciences, USA* **113**: 12322–12327.

Gibson DG, Young L, Chuang R-Y, Venter JC, Hutchison CA, Smith HO. 2009. Enzymatic assembly of DNA molecules up to several hundred kilobases. *Nature Methods* **6**: 343–345.

Gutekunst K, Chen X, Schreiber K, Kaspar U, Makam S, Appel J. 2014. The bidirectional NiFe-hydrogenase in *Synechocystis* sp. PCC 6803 is reduced by flavodoxin and ferredoxin and is essential under mixotrophic, nitrate-limiting conditions. *Journal of Biological Chemistry* **289**: 1930–1937.

Hanke GT, Satomi Y, Shinmura K, Takao T, Hase T. 2011. A screen for potential ferredoxin electron transfer partners uncovers new, redox dependent interactions. *Biochimica et Biophysica Acta (BBA) – Proteins and Proteomics.* **1814**: 366–374.

Helman Y, Tchernov D, Reinhold L, Shibata M, Ogawa T, Schwarz R, Ohad I, Kaplan A. 2003. Genes encoding a-type flavoproteins are essential for photoreduction of O_2 in cyanobacteria. *Current Biology* **13**: 230–235.

Hu C-D, Chinenov Y, Kerppola TK. 2002. Visualization of interactions among bZIP and Rel family proteins in living cells using bimolecular fluorescence complementation. *Molecular Cell* **9**: 789–798.

Hubáček M, Wey LT, Kourist R, Malihan-Yap L, Nikkanen L, Allahverdiyeva Y. 2024. Strong heterologous electron sink outcompetes alternative electron transport pathways in photosynthesis. *The Plant Journal* **20**: 789.

Imagawa T, Tsuge H, Sugimoto Y, Utsunomiya H, Yokoyama S, Kuramitsu S. 2005. RIKEN structural genomics/proteomics initiative (RSGI). *Tanpakushitsu Kakusan Koso* **20**: 4512.

Jackson PJ, Hitchcock A, Brindley AA, Dickman MJ, Hunter CN. 2023. Absolute quantification of cellular levels of photosynthesis-related proteins in *Synechocystis* sp. PCC 6803. *Photosynthesis Research* **155**: 219–245.

Johnson JE, Cornell RB. 1999. Amphitropic proteins: regulation by reversible membrane interactions (Review). *Molecular Membrane Biology* **16**: 217–235.

Jokel M, Johnson X, Peltier G, Aro E-M, Allahverdiyeva Y. 2018. Hunting the main player enabling *Chlamydomonas reinhardtii* growth under fluctuating light. *The Plant Journal* **94**: 822–835.

Joliot P, Joliot A. 2008. Quantification of the electrochemical proton gradient and activation of ATP synthase in leaves. *Biochimica et Biophysica Acta (BBA) - Bioenergetics* **1777**: 676–683.

Kerppola TK. 2008. Bimolecular fluorescence complementation (BiFC) analysis as a probe of protein interactions in living cells. *Annual Review of Biophysics* **37**: 465–487.

Klughammer C, Schreiber U. 2016. Deconvolution of ferredoxin, plastocyanin, and P700 transmittance changes in intact leaves with a new type of kinetic LED array spectrophotometer. *Photosynthesis Research* **128**: 195–214.

Kodama Y, Hu C-D. 2010. An improved bimolecular fluorescence complementation assay with a high signal-to-noise ratio. *BioTechniques* **49**: 793.

Korn A, Ajlani G, Lagoutte B, Gall A, Sétif P. 2009. Ferredoxin:$NADP^+$ oxidoreductase association with phycocyanin modulates its properties. *Journal of Biological Chemistry* **284**: 31789–31797.

Kozakov D, Hall DR, Xia B, Porter KA, Padhorny D, Yueh C, Beglov D, Vajda S. 2017. The ClusPro web server for protein–protein docking. *Nature Protocols* **12**: 255–278.

Kudla J, Bock R. 2016. Lighting the way to protein–protein interactions: recommendations on best practices for bimolecular fluorescence complementation analyses. *Plant Cell* **28**: 1002–1008.

Lehtonen JV, Still D-J, Rantanen V, Ekholm J, Bjrklund D, Iftikhar Z, Huhtala M, Repo S, Jussila A, Jaakkola J *et al.* 2004. BODIL: a molecular modeling environment for structure-function analysis and drug design. *Journal of Computer-Aided Molecular Design* **18**: 401–419.

Li J, Hamaoka N, Makino F, Kawamoto A, Lin Y, Rögner M, Nowaczyk MM, Lee Y-H, Namba K, Gerle C *et al.* 2022. Structure of cyanobacterial photosystem I complexed with ferredoxin at 1.97 Å resolution. *Communications Biology* **5**: 951.

Liu H, Weisz DA, Zhang MM, Cheng M, Zhang B, Zhang H, Gerstenecker GS, Pakrasi HB, Gross ML, Blankenship RE. 2019. Phycobilisomes harbor FNR_L in cyanobacteria. *MBio* **10**: 789.

Mangan NM, Flamholz A, Hood RD, Milo R, Savage DF. 2016. pH determines the energetic efficiency of the cyanobacterial CO_2 concentrating mechanism. *Proceedings of the National Academy of Sciences, USA* **113**: E5354–E5362.

Marteyn B, Domain F, Legrain P, Chauvat F, Cassier-Chauvat C. 2009. The thioredoxin reductase-glutaredoxins-ferredoxin crossroad pathway for selenate tolerance in *Synechocystis* PCC6803. *Molecular Microbiology* **71**: 520–532.

Miller NT, Ajlani G, Burnap RL. 2022. Cyclic electron flow-coupled proton pumping in *Synechocystis* sp. PCC6803 is dependent upon NADPH oxidation by the soluble isoform of ferredoxin:NADP-Oxidoreductase. *Microorganisms.* **10**: 855.

Mirdita M, Schütze K, Moriwaki Y, Heo L, Ovchinnikov S, Steinegger M. 2022. ColabFold: making protein folding accessible to all. *Nature Methods* **19**: 679–682.

Mulgrew-Nesbitt A, Diraviyam K, Wang J, Singh S, Murray P, Li Z, Rogers L, Mirkovic N, Murray D. 2006. The role of electrostatics in protein–membrane interactions. *Biochimica et Biophysica Acta (BBA) – Molecular and Cell Biology of Lipids* **1761**: 812–826.

Mustila H, Allahverdiyeva Y, Isojarvi J, Aro EM, Eisenhut M. 2014. The bacterial-type [4Fe-4S] ferredoxin 7 has a regulatory function under photooxidative stress conditions in the cyanobacterium *Synechocystis* sp. PCC 6803. *Biochimica et Biophysica Acta, Bioenergetics* **1837**: 1293–1304.

Mustila H, Paananen P, Battchikova N, Santana-Sanchez A, Muth-Pawlak D, Hagemann M, Aro E-M, Allahverdiyeva Y. 2016. The flavodiiron protein Flv3 functions as a homo-oligomer during stress acclimation and is distinct from the Flv1/Flv3 hetero-oligomer specific to the O-2 photoreduction pathway. *Plant & Cell Physiology* **57**: 1468–1483.

Nikkanen L, Hubacek M, Allahverdiyeva Y. 2021a. 10 Photosynthetic microorganisms as biocatalysts. In: Rögner M, ed. *Photosynthetic*. Berlin, Germany: De Gruyter, 257–278.

Nikkanen L, Santana Sánchez A, Ermakova M, Rögner M, Cournac L, Allahverdiyeva Y. 2020. Functional redundancy between flavodiiron proteins and NDH-1 in *Synechocystis* sp. PCC 6803. *The Plant Journal* **103**: 1460–1476.

Nikkanen L, Solymosi D, Jokel M, Allahverdiyeva Y. 2021b. Regulatory electron transport pathways of photosynthesis in cyanobacteria and microalgae: recent advances and biotechnological prospects. *Physiologia Plantarum* **173**: 514–525.

Nikkanen L, Toivola J, Rintamäki E. 2016. Crosstalk between chloroplast thioredoxin systems in regulation of photosynthesis. *Plant, Cell & Environment* **39**: 1691–1705.

Ohkawa H, Pakrasi HB, Ogawa T. 2000. Two types of functionally distinct NAD(P)H dehydrogenases in *Synechocystis* sp. strain PCC6803. *Journal of Biological Chemistry* **275**: 31630–31634.

Ortega-Martínez P, Nikkanen L, Wey LT, Florencio FJ, Allahverdiyeva Y, Díaz-Troya S. 2024. Glycogen synthesis prevents metabolic imbalance and disruption of photosynthetic electron transport from photosystem II during transition to photomixotrophy in *Synechocystis* sp. PCC 6803. *New Phytologist* **243**: 162–179.

Poncelet M, Cassier-Chauvat C, Leschelle X, Bottin H, Chauvat F. 1998. Targeted deletion and mutational analysis of the essential (2Fe-2S) plant-like ferredoxin in *Synechocystis* PCC6803 by plasmid shuffling. *Molecular Microbiology* **28**: 813–821.

Robert X, Gouet P. 2014. Deciphering key features in protein structures with the new ENDscript server. *Nucleic Acids Research* **42**: W320–W324.

Santana-Sánchez A, Nikkanen L, Werner E, Tóth G, Ermakova M, Kosourov S, Walter J, He M, Aro E, Allahverdiyeva Y. 2023. Flv3A facilitates O_2 photoreduction and affects H_2 photoproduction independently of Flv1A in diazotrophic Anabaena filaments. *New Phytologist* **237**: 126–139.

Santana-Sanchez A, Solymosi D, Mustila H, Bersanini L, Aro E-M, Allahverdiyeva Y. 2019. Flavodiiron proteins 1-to-4 function in versatile combinations in O-2 photoreduction in cyanobacteria. *eLife* **8**: e45766.

Schorsch M, Kramer M, Goss T, Eisenhut M, Robinson N, Osman D, Wilde A, Sadaf S, Brueckler H, Walder L *et al.* 2018. A unique ferredoxin acts as a player in the low-iron response of photosynthetic organisms. *Proceedings of the National Academy of Sciences, USA* **115**: E12111–E12120.

Schreiber U, Klughammer C. 2009. New NADPH/9-AA module for the DUAL-PAM-100: description, operation and examples of application. *PAM Application Notes* **2**: 1–13.

Schrödinger. 2022. *Schrödinger release 2022–3: desmond molecular dynamics system*. New York, NY, USA: Schrödinger.

Schrödinger Release 2023-1. 2021a. *BioLuminate*. New York, NY, USA: Schrödinger.

Schrödinger Release 2023-1. 2021b. *Maestro*. New York, NY, USA: Schrödinger.

Seedorf H, Hagemeier CH, Shima S, Thauer RK, Warkentin E, Ermler U. 2007. Structure of coenzyme F420H2 oxidase (FprA), a di-iron flavoprotein from methanogenic Archaea catalyzing the reduction of O_2 to H_2O. *FEBS Journal* **274**: 1588–1599.

Sétif P, Shimakawa G, Krieger-Liszkay A, Miyake C. 2020. Identification of the electron donor to flavodiiron proteins in *Synechocystis* sp. PCC 6803 by *in vivo* spectroscopy. *Biochimica et Biophysica Acta (BBA) – Bioenergetics* **1861**: 148256.

Shimakawa G, Shaku K, Nishi A, Hayashi R, Yamamoto H, Sakamoto K, Makino A, Miyake C. 2015. FLAVODIIRON2 and FLAVODIIRON4 proteins mediate an oxygen-dependent alternative electron flow in *Synechocystis* sp PCC 6803 under CO_2-limited conditions. *Plant Physiology* **167**: 472–U732.

Shimakawa G, Shoguchi E, Burlacot A, Ifuku K, Che Y, Kumazawa M, Tanaka K, Nakanishi S. 2022. Coral symbionts evolved a functional polycistronic flavodiiron gene. *Photosynthesis Research* **151**: 113–124.

Stauffer W, Sheng H, Lim HN. 2018. EzColocalization: an ImageJ plugin for visualizing and measuring colocalization in cells and organisms. *Scientific Reports* **8**: 15764.

Storti M, Puggioni MP, Segalla A, Morosinotto T, Alboresi A. 2020. The chloroplast NADH dehydrogenase-like complex influences the photosynthetic activity of the moss *Physcomitrella patens*. *Journal of Experimental Botany* **71**: 5538–5548.

Teuber M, Rogner M, Berry S. 2001. Fluorescent probes for non-invasive bioenergetic studies of whole cyanobacterial cells. *Biochimica et Biophysica Acta–Bioenergetics* **1506**: 31–46.

Theune ML, Hildebrandt S, Steffen-Heins A, Bilger W, Gutekunst K, Appel J. 2021. *In-vivo* quantification of electron flow through photosystem I – cyclic electron transport makes up about 35% in a cyanobacterium. *Biochimica et Biophysica Acta (BBA) – Bioenergetics* **1862**: 148353.

Thiel K, Mulaku E, Dandapani H, Nagy C, Aro EM, Kallio P. 2018. Translation efficiency of heterologous proteins is significantly affected by the genetic context of RBS sequences in engineered cyanobacterium *Synechocystis* sp. PCC 6803. *Microbial Cell Factories* **17**: 34.

Thomas J-C, Ughy B, Lagoutte B, Ajlani G. 2006. A second isoform of the ferredoxin:NADP oxidoreductase generated by an in-frame initiation of translation. *National Academy of Sciences, USA* **103**: 18368–18373.

Vicente JB, Gomes CM, Wasserfallen A, Teixeira M. 2002. Module fusion in an A-type flavoprotein from the cyanobacterium *Synechocystis* condenses a multiple-component pathway in a single polypeptide chain. *Biochemical and Biophysical Research Communications* **294**: 82–87.

Viola S, Bailleul B, Yu J, Nixon P, Selles J, Joliot P, Wollman F-A. 2019. Probing the electric field across thylakoid membranes in cyanobacteria. *Proceedings of the National Academy of Sciences, USA* **116**: 21900–21906.

Walter M, Chaban C, Schutze K, Batistic O, Weckermann K, Nake C, Blazevic D, Grefen C, Schumacher K, Oecking C *et al.* 2004. Visualization of protein interactions in living plant cells using bimolecular fluorescence complementation. *The Plant Journal* **40**: 428–438.

Wang Y, Chen X, Spengler K, Terberger K, Boehm M, Appel J, Barske T, Timm S, Battchikova N, Hagemann M *et al.* 2022. Pyruvate:ferredoxin oxidoreductase and low abundant ferredoxins support aerobic photomixotrophic growth in cyanobacteria. *eLife* **11**: 459.

Webb B, Sali A. 2016. Comparative protein structure modeling using Modeller. *Current Protocols in Bioinformatics* **54**: 1330.

Williams JGK. 1988. Construction of specific mutations in Photosystem-II Photosynthetic Reaction Center by genetic-engineering methods in *synechocystis*-6803. *Methods in Enzymology* **167**: 766–778.

Yokoo R, Hood RD, Savage DF. 2015. Live-cell imaging of cyanobacteria. *Photosynthesis Research* **126**: 33–46.

Zhang P, Allahverdiyeva Y, Eisenhut M, Aro E-M. 2009. Flavodiiron proteins in oxygenic photosynthetic organisms: photoprotection of photosystem II by Flv2 and Flv4 in *Synechocystis* sp. PCC 6803. *PLoS ONE* **4**: e5331.

Zhang P, Eisenhut M, Brandt A-M, Carmel D, Silen HM, Vass I, Allahverdiyeva Y, Salminen TA, Aro E-M. 2012. Operon flv4-flv2 provides cyanobacterial photosystem ii with flexibility of electron transfer. *Plant Cell* **24**: 1952–1971.

Supporting Information

Additional Supporting Information may be found online in the Supporting Information section at the end of the article.

Fig. S1 Plasmid map of a BiFC construct to express *Synechocystis flv1* and *petF* (Fed1) as fusion proteins with N- and C-terminal Venus fragments, respectively.

Fig. S2 Characterisation of Fed mutants.

Fig. S3 'Empty' vector control experiments for BiFC.

Fig. S4 O_2 evolution, O_2 uptake, and CO_2 fixation in ΔFlv3 and ΔFNR mutant strains.

Fig. S5 NAD(P)H fluorescence changes under 3% [CO_2] and low irradiance.

Fig. S6 Redox kinetics of PSI electron carriers in WT, ΔFlv3, ΔFNR_L, and ΔFNR_S cells.

Fig. S7 BiFC tests between FNR and Flv2.

Fig. S8 Verification of expression of BiFC fusion constructs by immunoblotting.

Fig. S9 Redox changes of PC, P700, and Fed in WT, ΔFed, and ΔFlv3 cells.

Fig. S10 BiFC test for interaction between Flv3-VN and Fed1-VC.

Fig. S11 BiFC tests for interactions between Fed9 and Flv1 or Flv3.

Fig. S12 Differently localising subpopulations of Flv1-VN/Flv3-VC and Flv2-VC/Flv4-VN interactions in BiFC.

Fig. S13 Effect of CCCP on the *pmf* in *Synechocystis*.

Fig. S14 Generation of the *pmf*, thylakoid conductivity (gH+), and proton flux (vH+) during dark-to-light transitions in low vs high cation concentration.

Fig. S15 Effect of nigericin and DCMU on ΔpH generation during induction of photosynthesis.

Fig. S16 Effect of nigericin on the subcellular localisation of Flv1/3 and Flv2/4 interactions.

Fig. S17 Effect of DCMU on the subcellular localisation of Flv1/3 and Flv2/4 interactions.

Fig. S18 Immunodetection of the subcellular localisation of FDPs.

Fig. S19 Effect of CCCP on O_2 uptake.

Fig. S20 Effect of nigericin on photosynthesis.

Fig. S21 Cytosolic alkalisation upon illumination.

Fig. S22 Effect of DTT, $CuCl_2$, and KCN on photosynthesis.

Fig. S23 Effect of DTT, $CuCl_2$, and KCN on the subcellular localisation of Flv2/4 interactions.

Fig. S24 Effect of DTT, $CuCl_2$, and KCN on the subcellular localisation of Flv1/3 interactions.

Fig. S25 Effect of cation concentration on the subcellular localisation of Flv1/3 and Flv2/4 interactions.

Fig. S26 BiFC tests for Flv1 and Flv3 self-interactions and between Flv2 and Flv3.

Fig. S27 Effect of cation concentration and *pmf* uncoupling on the subcellular localisation of Flv3 self-interactions.

Fig. S28 *In silico* analysis of electrostatic surface charges of FDP monomers under pH 7.0 and pH 8.5.

Methods S1 Modular cloning to obtain BiFC strains.

Table S1 Primers used for generating the ΔFed10 and ΔFed11 strains.

Table S2 Results from statistical tests in the main article.

Table S3 Results from statistical tests in Supporting Information.

Please note: Wiley is not responsible for the content or functionality of any Supporting Information supplied by the authors. Any queries (other than missing material) should be directed to the *New Phytologist* Central Office.

Disclaimer: The New Phytologist Foundation remains neutral with regard to jurisdictional claims in maps and in any institutional affiliations.